Micro-CT image acquisition, processing, and segmentation to track lung cancer progression and characterise pulmonary nodules in mice

May Zaw Thin[1,2,9*], Christopher Moore[3,9], Thomas Snoeks[4], Tammy Kalber[5], Julian Downward[3,6*], Axel Behrens[1,2,7,8]

[1]Cancer Stem Cell Laboratory, Institute of Cancer Research, 237 Fulham Road, London SW3 6JB, UK

[2]Adult Stem Cell Laboratory, The Francis Crick Institute, 1 Midland Road, London, NW1 1AT, UK.

[3]Oncogene Biology Laboratory, The Francis Crick Institute, 1 Midland Road, London NW1 1AT, UK

[4]Imaging Research Facility, The Francis Crick Institute, 1 Midland Road, London NW1 1AT, UK

[5]Centre for Advanced Biomedical Imaging (CABI), University College London, Paul O'Gorman Building, WC1E 6DD, London, UK

[6]Lung Cancer Group, Division of Molecular Pathology, Institute of Cancer Research, 237 Fulham Road, London SW3 6JB, UK

[7]Department of Surgery and Cancer, Imperial College London, London SW7 2AZ, UK

[8]Convergence Science Centre, Imperial College London, South Kensington Campus, London SW7 2AZ, UK

[9]Equal contribution

*Corresponding authors: Julian.Downward@crick.ac.uk, may.zawthin@icr.ac.uk

Editorial Summary: A micro computed X-ray tomography-based approach for quantifying the number and volume of lung cancer nodules over time, enabling the tracking of individual nodule formation, tumour growth and response to therapy.

Twitter suggestion: Longitudinal tracking and radiological characterisation of lung cancer nodules via micro computed X-ray tomography

Key references

1. Castellano, E. *et al.* Requirement for interaction of PI3-kinase p110α with RAS in lung tumor maintenance. *Cancer Cell* **24**, 617-630, doi:10.1016/j.ccr.2013.09.012 (2013).
2. Molina-Arcas, M. *et al.* Development of combination therapies to maximize the impact of KRAS-G12C inhibitors in lung cancer. *Sci Transl Med* **11**, doi:10.1126/scitranslmed.aaw7999 (2019).

3. van Maldegem, F. *et al.* Characterisation of tumour microenvironment remodelling following oncogene inhibition in preclinical studies with imaging mass cytometry. *Nature Communications* **12**, 5906, doi:10.1038/s41467-021-26214-x (2021).

Abstract

X-ray computed tomography is a reliable technique for the detection and longitudinal monitoring of pulmonary nodules. In preclinical stages of diagnostic or therapeutic development, the miniaturised versions of the clinical CT scanners, are ideally suited for carrying out translationally relevant research in conditions which closely mimic those found in the clinic. In this Protocol, we provide image acquisition parameters optimised for low radiation dose, high-resolution and high-throughput CT imaging using three commercially available micro-computed tomography scanners, together with a detailed description of the image analysis tools required to identify a variety of lung tumour types, characterised by specific radiological features. For each animal, image acquisition takes 4 - 8 minutes, and data analysis typically requires 10 - 30 minutes. Researchers with basic training in animal handling, medical imaging and software analysis should be able to implement this protocol across a wide range of lung cancer models in mice for investigating the molecular mechanisms driving lung cancer development and the assessment of diagnostic and therapeutic agents.

Key words

Micro-CT, lung, cancer, 3D, *in vivo* imaging

Introduction

Lung cancer is the leading cause of cancer-related mortality worldwide affecting an estimated 1.8 million deaths per year[1]. Animal models of lung cancer play an important role in researching therapies by elucidating the mechanisms regulating the development of lung cancer and can be adopted in the preclinical phase of drug discovery, to test the ability of lead compounds to reduce the growth of a tumour. In preclinical studies, *ex vivo* histological analysis is routinely applied to assess therapeutic response. However, the lack of longitudinal information on tumour growth, reduction, or growth arrest, in addition to the large numbers of animals per cohort required by histology-based methods due to significant inter-animal variation, limit the utility of such data from a translational standpoint. Unlike histology-based approaches, non-invasive *in vivo* imaging allows serial monitoring of the same animal over time, which in turn enables a quantitative or semi-quantitative assessment of otherwise unknown variables such as tumour onset (by detecting the early stages of mass formation), progression (by detecting changes in tumour size), and therapy response (by detecting tumour shrinkage or growth arrest). Non-invasive *in vivo* imaging is advantageous to experimental design as it reduces the number of animals needed in each cohort and thereby allowing to better account for, or even directly measure, inter-animal variability[2].

X-ray computed tomography (CT) is a widely available diagnostic imaging modality which uses an X-ray beam to create a cross-sectional tomographic plane of the body. CT measures the electron density of the tissue by calculating the attenuation coefficient of the X-ray beam as it travels through the animal from data acquired by a detector array. The X-ray source and the detectors typically rotate around the body on a gantry while the animal remains sedated at its centre. A series of cross-sectional 2D slices is then reconstructed into 3D digital format with each pixel representing a measurement of attenuation coefficient or density of the tissue which the X-ray beam passes through. The measurement is expressed in Hounsfield Units (HU) using water as a zero threshold on the scale[3]. The range and variation of HU values for different types of tissues, as extensively discussed in the literature[4,5]. Generally, tissues denser than water, such as muscle and liver, are assigned positive HU numbers with high density (compact bone having +1000 HU), whereas tissues less dense than water, such as adipose tissue, are assigned negative HU numbers. Air displays extremely low density and is associated with -1000 HU. Therefore, in a greyscale CT image of the chest, the lung which is full of air appears dark, soft tissue or tumour nodules are grey and the ribs and the vertebrae of the spine are white.

Due to its excellent air-tissue contrast, CT is the most frequently used imaging technique in the clinic for lung cancer screening and therapy monitoring[6]. In preclinical research, micro-CT

125 scanners are frequently used for lung imaging[7,8,9,10,11]. Micro-CT scanners are miniaturised
126 versions of their clinical counterparts, where the size of the gantry, bed and detectors are
127 tailored for small animals. Its use to study different types of lung cancer models has
128 nevertheless remained technically challenging due to motion artefacts (in particular chest and
129 lung expansions during breathing), the lack of documentation of detailed radiological
130 characteristics of each tumour type and a lack of robust analysis tools. The lack of a structured
131 and internationally recognised protocol to standardise *in vivo* preclinical imaging data
132 acquisition and analysis pipelines hinders the direct comparison of datasets acquired via
133 different instruments or even different users, hence reducing the reproducibility of research
134 findings in the field. Here, we present an optimised protocol for *in vivo* micro-CT imaging
135 setups and analysis tools for mouse models of lung cancer. This approach offers a simple to
136 implement and non-invasive method for accurate identification of lung tumour nodules and
137 enables the serial quantification of tumour and lung volume changes in response to a wide
138 range of genetic or therapeutic interventions.
139
140 **Development of the protocol**
141 The system design of the *in vivo* micro-CT is similar to the clinical scanner in which the gantry
142 mounted with the X-ray source and detectors rotates around the animal. However, the
143 scanning efficiency of a micro-CT scanner is lower than that possible with a clinical instrument,
144 as smaller devices trade efficiency for a higher image resolution, typically <100 μm[12]. The
145 choice of CT imaging parameters also needs to strike a balance between the radiation dose
146 and the desired spatial resolution. Small animals have fast respiratory and cardiac rates (adult
147 mice values range between heart rates of 310-840 beats per minute and respiratory rates of
148 80-230 breaths per minute), which pose a challenge for lung imaging. Bearing in mind that
149 both rate values significantly slow down under anaesthesia, the motion can be accounted for
150 using either prospective gating or retrospective gating. Although prospective gating can
151 provide images with better resolution and fewer motion artefacts[13], the commercially available
152 micro-CT scanners are not equipped with x-ray shutters triggered by respiration motion,
153 leading to long scan acquisition timeframes. Retrospective gating is thus preferred for shorter
154 scan times which help lower radiation exposure[14,15].
155 To facilitate reproducibility across scanners and users, we have developed a set of CT
156 acquisition parameters at low x-ray dose and tested these in two standalone micro-CT
157 scanners and a preclinical multimodal positron emission tomography (PET) and CT
158 instrument. Our protocol provides straightforward image acquisition steps with robust tumour
159 analysis tools which can be easily adapted to a wide range of lung tumour types. We have
160 obtained reliable and reproducible results with various tumour models, including genetically
161 engineered mice[8,9,16,17], systemic cell injections through the tail vein[18], a urethane-induced

162 lung tumour[9], as well as orthotopic intratracheal cell transplantations[7], achieving high
163 resolution images of small lung nodules (0.06 – 0.08 mm^3) and tracking individual tumours
164 over time without using contrast agents. Our analysis methods were optimised after noticing
165 that the analysis manual provided by the manufacturers of the scanners, resulted in
166 inconsistencies in tumour volume quantification between radiological phenotypes. Thus, we
167 developed a set of analysis methods suitable for each radiological feature which are
168 performed with commercially available software such as Bruker's CTAn and Analyze software,
169 widely available to the preclinical imaging community.
170
171 **Applications**
172 Micro-CT imaging enables researchers to study *in vivo* lung tumour initiation and development
173 in a pathophysiologically relevant context. Serial CT imaging and total tumour volume
174 analyses offer a non-invasive way of quantifying tumour burden with a strong correlation with
175 standard histopathological assessments[11,19,20]. We have applied our image acquisition and
176 tumour volume analysis protocols for determining the Ras protein interaction in KRAS-driven
177 lung tumours[7] and for evaluating the efficacy of KRAS-G12C inhibitors[9,21]. In addition, tracking
178 individual tumour nodules over time can be used to detect the emergence of nodule-specific
179 resistance to therapy in mutant EGFR-driven tumours[8]. Assessing lung volume changes can
180 help shed light on the mechanisms driving compensatory lung volume expansion in infectious
181 lung diseases[22] and lung metastasis[23].
182 We have applied our image acquisition protocols to assess radiological characteristics
183 displayed by the tumour nodules in multiple lung tumour models. For example, in KRAS-driven
184 autochthonous tumour models (i.e., Cre-recombinase mediated expression of $KRAS^{G12D}$ and
185 *p53* loss of function)[9,17,24], several localised nodules (**Fig. 1a**) with smooth lobulated (**Fig. 1b**)
186 or spiculated margins (**Fig. 1c**) can be identified starting from ~6-8 weeks after the adenoviral
187 delivery of Cre-recombinase using intratracheal intubation[24]. Depending on the viral dose, on
188 average between 6 - 10 nodules per animal can be detected at 12 weeks after instillation. The
189 chemically-induced lung cancer model, for example, the administration of urethane (a known
190 carcinogen) induces $KRAS^{Q61R}$ mutations[25]. This model is less aggressive and has fewer
191 nodules than the Cre-recombinase controlled KRAS mutation models[9,25] but presents with the
192 similar radiological appearance (**Fig. 1d**). In an orthotopic model of intratracheal tumour cell
193 transplantation[7], multiple nodules with defined margins can be observed (**Fig. 1e**), however
194 the rate of tumour development between animals typically varies from ~12-16 weeks after cell
195 transplantation.
196 We have applied two types of tumour volume analyses depending on the radiological
197 phenotypes of tumour models. Individual nodule segmentation and total tumour volume
198 quantification are more suitable for tumour models with localised pulmonary nodules

199 compared to widespread diffuse nodules. For example, a doxycycline inducible autochthonous
200 mouse model of epidermal growth factor receptor (EGFR)^{L858R} -driven lung cancer[8,26,27] usually
201 presents a mixture of diffuse nodules with ground-glass appearances (**Fig. 1f-h**) and discrete
202 lesions (**Fig. 1i**). These lesions can be detected via micro-CT starting from the fourth week of
203 doxycycline administration. Similar radiological characteristics can be detected in models
204 developed by administering cancer cells via the tail vein (**Fig. 1j**), where the characteristics
205 vary depending on the type of cells and mouse strains used. In models with widespread diffuse
206 nodules, tumour burden can be indirectly measured by calculating lung (air inside the lung)
207 volume because individual tumour segmentation is very challenging to achieve accurately.
208
209 **Comparison with other methods**
210 A variety of commercially available non-invasive *in vivo* imaging instruments can be used for
211 the detection of lung cancer. The choice of which approach to use often depends on the
212 availability of the equipment and the departmental organisation (e.g., radiology or cancer
213 research) which runs the imaging suites. Magnetic resonance imaging (MRI) is a reliable
214 imaging method to monitor lung tumour growth[10,28]. However MRI requires longer scanning
215 time (~40 min per animal)[29] and provides lower resolution than CT. In addition, availability of
216 preclinical MRI scanners is limited due to its high cost. Optical imaging methods such as
217 fluorescence and bioluminescence imaging (BLI) are faster and more sensitive in detecting
218 lung tumours[28,30]. Nonetheless, the spatial resolution of optical imaging approaches is poor
219 and individual nodules are difficult to discriminate. In addition, *in vivo* fluorescence imaging
220 suffers from the background autofluorescence and relies on imaging in the near-infrared (NIR)
221 window using NIR probes[30,31] and far-red fluorescence protein expressing cells[32]. BLI also
222 requires the use of tumour models with luciferase expressing cells[31] and in genetically
223 engineered mouse models, it can be time consuming and technically complexed to couple
224 genetically encoded bioluminescent reporter with an oncogenic pathway of interest[33,34]. Single
225 photon emission computed tomography (SPECT) and positron emission tomography (PET)
226 can be used to detect lung cancers and can provide molecular and metabolic activity of
227 tumours[35-38], but their limitations are poor spatial resolution (≤1 mm in SPECT[39] and >1 mm in
228 PET)[40], long scanning time and require the use of radioisotopes. Depending on the amount of
229 radioactivity injected, the scanning time for SPECT imaging is 10 – 50 min per animal[41-43] and
230 PET imaging is 15 – 60 min per animal[44-47].To co-register detailed anatomical localisation with
231 molecular information, commercial small animal SPECT (e.g., nanoScan SPECT/CT, Mediso),
232 PET (e.g., nanoScan PET/CT, Mediso) and optical (e.g., IVIS SpectrumCT, PerkinElmer)
233 imaging scanners are usually integrated x-ray CT inside the same imaging gantry or platform.
234 Therefore, further optimisation of our protocol in multimodal scanners may extend the use of
235 this protocol for imaging lung cancer. Micro-CT scanners have relatively straightforward

236 maintenance requirements (e.g., calibration of the x-ray tube), do not typically require contrast
237 agents (because the tissue/air interface in the lung provides high contrast) and are
238 inexpensive to operate, making them suitable for lung imaging.
239
240 **Limitations**
241 The main limitation of micro-CT imaging is the exposure to ionizing radiation, which, over time
242 (when used to serially image the same animal), could cause radiation-induced lung injury and
243 confound the imaging read-outs. However, radiation doses delivered with serial micro-CT of
244 animals (average 840 mGy for a single scan) are an order of magnitude lower than the typical
245 doses (4 – 20 Gy) applied in the field of radiotherapy[48,49]. Based on our regulated use of the
246 protocol (see the Regulatory Approvals section) with various lung tumour models and different
247 micro-CT scanners, we have not observed any radiation-induced adverse effects or tumour
248 volume changes, consistent with other studies[49-51]. CT is a high-resolution technique for
249 anatomical information, but it cannot provide molecular information without targeted contrast
250 agents, such as that provided by targeted gold nanoparticles[52]. The feasibility of using micro-
251 CT for imaging squamous cell lung cancer models has not been assessed using this protocol
252 due to the lack of well characterised *in vivo* mouse models. It is useful to note that the majority
253 of autochthonous murine models of lung cancer display a mixture of adenocarcinoma and
254 squamous cell carcinoma[53-56], our CT imaging protocol cannot conclusively disambiguate
255 between the two.
256 Although our simple, easily adaptable analysis tool can provide accurate measurements of
257 lung and tumour volume, it is mainly based on a semi-automated segmentation strategy which
258 is more laborious than complex automated methods[57] or deep learning-based approaches[58].
259 The accuracy and reliability of deep learning tools have yet to be validated across multiple
260 lung tumour models. We envisage that our protocol could therefore also serve as a tool to
261 improve the efficiency of automated segmentation methods. Our lung segmentation tools are
262 based on density-based thresholding, therefore are not suitable for discriminating between
263 pulmonary vessels, necrotic tissues, and tumours, which all have a similar density. However,
264 we and others who used similar strategies have shown that tumour burden measurement from
265 CT strongly correlates with histological assessments[7,8,59,60]. The possible explanation is that
266 the intrapulmonary vessels and the necrotic tissues represent a relatively small part of the soft
267 tissue, and their incorporation does not have a notable difference in evaluation of therapy and
268 genetic intervention.
269
270 **Experimental design**
271 The protocol and steps here are optimised for the commercially available Skyscan 1176
272 (Bruker), the Quantum GX2 (PerkinElmer) micro-CT scanners and the nanoScan PET/CT

273 (Mediso) system. Our protocol could be adapted to other micro-CT scanners with similar
274 specifications. The image acquisition steps outlined here are straightforward and researchers
275 with no prior experience in CT lung imaging can easily apply it to their relevant research
276 projects. The image analysis tools described here are simple yet robust and easily adjustable
277 depending on the radiological phenotypes of the model. No MATLAB or programming
278 experience is required. All analyses are performed with two commercially available software
279 packages: Bruker's CTAn and Analyze which are part of software packages for Skyscan and
280 Quantum GX2 respectively. We have applied our protocol in several lung tumour models, for
281 example, Kras mutant model, doxycycline inducible EGFR mutant model, tail vein injection
282 model, urethane-induced model and intratracheal cell transplantation model. The protocol
283 presented here can be applied in other mouse models of lung cancer not limited to the models
284 that we provided as examples. We have used both male and female mice from different lung
285 cancer models and we have observed no sex differences in tumour engraftment, growth rate
286 and micro-CT imaging parameters, e.g., radiation side effect.
287 **Figure 2** shows the overview of the Procedure: following a series of animal preparation and
288 image acquisition steps (Steps 1-15), respiratory gating and reconstruction steps (Steps 16-
289 17) are explained in order to obtain good quality images for image analysis steps (Steps 18-
290 22). Generally, there are two types of tumour volume analysis which can be performed: the
291 direct measurement of individual tumour volume or the indirect quantification of tumour growth
292 based on loss of air (healthy lung) volume depending on the radiological phenotype of the
293 tumours and the research questions being asked. Our analysis pipeline is mainly based on
294 the semiautomatic segmentation of images following the application of an intensity threshold
295 value and the selection of regions of interests and image processing (see steps 23-28 for
296 detail); however, the automated segmentation steps and analysis of lung volume with the
297 Analyze software use the surrounding organs as calibrators (see step 28B for detail).
298 For studies with genetic (e.g., CreERT2-mediated genetic deletion via tamoxifen
299 administration)[7] or therapeutic intervention, a baseline scan should be performed on the day
300 before or the first day of treatment. Depending on the tumour development stage and
301 treatment approach, longitudinal scans should be performed weekly, twice, or once per month.
302 We ensure that all experimental groups receive the same number of scans but no more than
303 5 times per month to avoid radiation side effects. Before investing time, money, and animals
304 on one model, we advise researchers to review the radiological characteristic of the chosen
305 animal model and determine its suitability for their research objectives. For example, a mouse
306 model with diffuse, multiple lung tumours is not appropriate for identifying a specific lesion
307 resistance to targeted therapy. Bearing in mind that a quantitative tumour volume (e.g., in
308 mm^3) assessment can take up to 30 min per mouse, the total number of tumours (e.g., 10

309 nodules) detected per animal (see steps 18-22 for detail) can be used as a rapid (up to 15 min
310 per mouse), qualitative evaluation of tumour burden for creating different treatment groups.
311
312 **Regulatory approvals**
313
314 All micro-CT studies described in this protocol are in compliance with the Ionising Radiation
315 Regulations 2017 (IRR17). The Francis Crick Institute and the University College London
316 enforce the Ionising Radiation Medical Exposure Regulations and follow the guidelines for the
317 use of radiation in medical research.
318
319 **Materials**
320 **Reagents**
321 • Gibco™ Fetal Bovine Serum (FBS), qualified, heat inactivated, E.U.-approved, South
322 America Origin (Fisher Scientific, cat. no. 10500064)
323 • Dulbecco's PBS, no calcium, no magnesium (Thermo Fisher Scientific, cat. no.
324 14190094)
325 • Gibco™ DMEM, high glucose (Fisher Scientific, cat. no. 11574486)
326 • Gibco™ L-glutamine (200 mM, Fisher Scientific, cat. no. 11539876)
327 • Penicillin and streptomycin (10,000 units penicillin and 10 mg streptomycin per mL in
328 0.9% NaCl, Sigma-Aldrich, cat. no. P0781)
329 • KPB6 (Cell Services at the Francis Crick Institute; RRID: CVCL_C0RJ)
330 **! Caution**
331 Cell culture should be checked regularly to ensure that cells are authentic and free
332 from mycoplasma infection.
333 • Isoflurane (IsoFlo, Zoetis, cat. no. NDC 0044-5260-05)
334 • Lubrithal ophthalmic soothing eye gel (10 g, Dechra)
335 • 3M™ Transpore™ surgical tape (3M ID 7100227485)
336 • Adenovirus expressing Cre-recombinase (Viral Vector Core, U of Iowa-5 Ad5CMVCre,
337 Plasmid: G0166 pAd5CMVCreMT1pA)
338 **! Caution**
339 Handling and administration of viruses should take place in the class 2 biosafety hood.
340 • Doxycycline-containing diet (Harlan-Teklad, cat. no. TD.01306, irradiated)
341 **! Caution**
342 To avoid accidental exposure to doxycycline, handle the food by using appropriate
343 personal protective equipment: gloves, mask, and lab coat.
344 • Urethane ≥99% (Sigma-Aldrich, cat. no. U2500)
345 **! Caution**

Toxic. May cause cancer. Work under a fume hood. Handle with care and appropriate personal protective equipment: gloves, mask, lab coat and protective goggles. Do not let product enter drains and dispose as required by local regulations.

- 22G (blue) catheter (25 mm, BD Insyte, cat. no. 381223)

Animals

All animal studies were approved by the Francis Crick Institute and the University College London Animal Ethics Committee and licensed under the UK Home Office regulations and the Guidance for the Operation of Animals (Scientific Procedures) Act 1986 (Home Office, London, United Kingdom) including Amendment Regulations 2012 and United Kingdom Coordinating Committee on Cancer Research Guidelines for the Welfare and Use of Animals in Cancer Research[61]. The protocol presented here can be used with both males and females.

Mouse models of lung cancer

***Kras* mutant model**

Kras$^{LSL\text{-}G12D/+}$; *Trp53*$^{Fl/Fl}$ (KP) mice were obtained from the Mouse Models of Human Cancer Consortium and mutant mice were generated as described previously[62]. In mixed-sex mice between 6-12 weeks of age and average weight of 25 g, lung tumours were initiated using intratracheal intubation of $1x10^6$ plaque forming units (pfu) adenovirus expressing Cre-recombinase (Viral Vector Core) as previously described[63]. Typically, lung tumours were first detected via micro-CT ~8 weeks after adeno-Cre infection.

Doxycycline inducible *EGFR* mutant model

The Clara cell secretory protein element - tetracycline-dependent activator (*CCSP-rtTA)* mice and *TetO-EGFR*^{L858R} mice were obtained from the Jackson Lab and Mouse Repository respectively, and the generation of both strains has been described previously[26,27]. In mixed-sex mice between 6-12 weeks of age and average weight of 25 g, tumour development is initiated by feeding mice with doxycycline-containing food pellets (625 ppm) continuously. Typically, lung tumours were first detected via micro-CT ~4 weeks after doxycycline administration.

IV injection model

KPB6, a murine lung adenocarcinoma cell line derived from KP mice (C57BL/6 background), was grown in DMEM supplemented with 10% FBS, 2 mM L-glutamine, 100 U/mL penicillin and 100 µg/mL streptomycin. 1 x 10^5 KPB6 cells were injected intravenously into the tail vein of 8-12-week-old C57BL/6 mice (mixed-sex) with average weight of 25 g. In our experience, lung tumours were first detected via micro-CT ~2 weeks after injection.

383

384 **Urethane-induced model**

385 Tumours were induced in 8-16-week-old mixed-sex FVB/NJ mice (25 – 30 g) by giving them
386 a single intraperitoneal injection of 1 g/kg of urethane in PBS. Lung tumours were first detected
387 via micro-CT ~16 weeks after urethane injection.

388

389 **Intratracheal cell transplantation model**

390 8-12-week-old mixed-sex C57BL/6 mice (25 – 30 g) were anaesthetized and 1 x 10^5 KPB6
391 cells per 50 µl of PBS were introduced directly into the lungs through the intratracheal catheter.
392 Lung tumours were first detected via micro-CT ~12-16 weeks after cell transplantation.

393

394 **Equipment**

395 - Skyscan 1176 (Bruker)
396 - Quantum GX2 (PerkinElmer)
397 - nanoScan PET/CT (Mediso)
398 - Perkin Elmer Rodent Anaesthesia System RAS-4
399 - Induction chamber (Vet Tech, cat no. AN010R)
400 - Isoflurane vaporiser (Vet Tech, cat no. AN003A)
401 - Oxygen concentrator (NIDEK Nuvo Lite 5LPM)
402 - Scavenger (Harvard Apparatus FLUOVAC Anaesthesia System, cat no. MA1 34-0388)
403 - Chamber warmer (EZ anaesthesia corporation, cat no. HB-163)
404 - Small animal recovery chamber (Vet Tech, cat no. HE010)

405 **Computer & Software**

406 - Image processing and analysis were performed using a dedicated imaging workstation
407 with the following specifications: processor: Intel® Xeon® W-2223 3.6GHz; memory:
408 128GB; SSD: 960 EVO 1TB; HDD Dell 1TB 7.2K SATA; OS: Windows 11; GPU:
409 NVIDIA GeForce GTX 1080 Ti.
410 - Data from Skyscan were analysed using CTAn software version 1.18 and 3D
411 visualisation was performed using CTVol software version 2.3.1.0 from Bruker.
412 - Data from Quantum GX2 were analysed and visualised in 3D using Analyze software
413 version 12.0 from AnalyzeDirect.
414 - Data from nanoScan PET/CT were analysed using CTAn software after converting to
415 compatible file format.

416

417 **Equipment setup**

All CT scanners require the X-ray source to warm up before scanning can take place. This process is only required once a day and the duration is 15 – 30 minutes depending on the type of scanner. To ensure a good quality image, we recommend regular calibration of Hounsfield units, CT gain and scanner alignment.

For Skyscan users, to have a uniform background image for the detector, flat field correction must be performed before a day's scanning. The following parameters need to be checked before flatfield correction: the status of X-ray source and current, correct pixel size and filter selected for lung scan and no object inside field of view (FOV).

Procedure

Animal preparation. Timing ~5-8 min

! Caution

All experiments involving live animals must follow local, national, and institutional guidelines.

1. Line the induction chamber with paper towel and fill it with 4% isoflurane.
2. Anaesthetise the mouse by placing inside the induction chamber and wait ~2 min until the mouse has lost its righting reflex and the breathing rate has become slower and deeper. ▲ **CRITICAL STEP** The mouse must be fully sedated before moving it to the bed.
3. When the mouse is unconscious, transfer it to the bed.

   Troubleshooting
4. Turn isoflurane vaporizer dial to 2% (for maintenance) with an oxygen flow rate of 0.5 - 1L/min.
5. Apply a drop of ophthalmic soothing eye gel over the eyeballs of the mouse to help keep the eyes moist. The gel lasts for the entire scanning duration (~10 min).
6. Place the mouse in a supine position with nose inside the nose cone (**Fig. 3a**) and secure the front paws gently to the bed using 3M transpore surgical tape to have a clear view of the lungs (**Fig. 3b**). ▲ **CRITICAL STEP** It is important to make sure that the front paws are not covering the chest and they are not within the scan field of view to reduce the motion artefact and streak artefact from the bone.
7. To ensure serial scans of the same animal display in the similar orientation, keep the body in midline and the spine straight.
8. Maintain the temperature of the animal using a hot air heater which is set at 37°C.
9. Monitor the respiratory rate using the video recording inside the scanner (Skyscan & Quantum GX2) or the respiration pad (nanoScan PET/CT).
10. Maintain respiratory rate at 40-50 breaths/min by adjusting the isoflurane flow rate (2.5 – 3% with an oxygen flow rate of 1L/min) and return to 2% when the respiratory rate reaches the desired range.

▲ **CRITICAL STEP** Isoflurane is an inhalational anaesthesia with variable sensitivity and adverse effects in different mouse strains. The level of isoflurane should be adjusted depending on the mouse strains used. Additionally, tumour burden in the lung will also affect anaesthesia induction and stable breathing rate. The higher the tumour burden in the lung, the greater the chance of the mouse having erratic breathing, resulting in bad quality images.

Troubleshooting

Image acquisition. Timing ~5-10 min

11. To position the mouse thorax within the scan field of view (FOV) (**Fig. 3c**), acquire the scout view in Skyscan and nanoScan PET/CT scanner or move the bed in Quantum GX2 scanner. ▲ **CRITICAL STEP** Before starting scanning, it is important to make sure that the whole lung is inside the FOV.

    Troubleshooting

12. Choose the scanning parameters depending on the type of micro-CT scanner (see **Table 1**).
13. When the scan is complete, remove the animal from the bed.
14. Place the animal in the heated recovery chamber (37°C). Recovery should occur rapidly with the mouse conscious after 2 minutes and fully recovered and mobile within 5 minutes.

    ! Caution

    Recovery of the mouse from anaesthesia will vary depending on strain and condition of the mouse. The greater the tumour burden, the longer the recovery time. If the mouse is breathing but not recovering from the anaesthesia after 20 minutes, or moving around very slowly, sacrifice of the mouse should be considered. It is important to make sure these adverse effects are described in the Home Office Project Licence and conform to relevant institutional guidelines.

15. Place the animal back into normal home cage together with its littermates for it to be returned to the animal housing facility.

Respiratory gating and reconstruction. Timing ~3-5 min

16. To reduce the motion artefact and improve the spatial resolution, sort the raw projection images into inspiration and expiration phases of respiratory cycle using the third party RespGate software[64] for Skyscan & nanoScan PET/CT scanner (option A) or in-built respiratory gating software for Quantum GX2 scanner (option B). End expiration phase is the most suitable for data analysis due to less respiration motion and better image quality.

492 (A) RespGate software – Skyscan & nanoScan PET/CT scanner
493 i. Open the raw projection images with RespGate software.
494 ii. Define the file path for saving gated data and then press start.
495 iii. Check the 'End expiration' box in software interface for gating.
496 iv. To track the upward (expiration) and downward (inspiration) movement of
497 the diaphragm, put medium sized square on the junction between lung and
498 diaphragm (one third over the diaphragm and two thirds over the lung) and
499 press left click on a mouse.
500 v. Repeat the same step (iv) for the eight different rotation angles of the raw
501 data. The software automatically presents these raw projection images
502 after each click and the gated data will be automatically processed at the
503 end.
504
505 (B) In-built respiratory gating software – Quantum GX2 scanner
506 i. To track the upward (expiration) and downward (inspiration) movement of
507 the diaphragm in each raw projection, place the green rectangle partially
508 over the diaphragm during the acquisition (Fig. 3c).
509 ii. At the end of image acquisition, the raw data will be automatically sort into
510 expiration and inspiration phases of respiratory cycle.
511 17. To reconstruct the gated data, choose the reconstruction parameters depending on
512 the type of CT scanner and software (see **Table 2**). **Figure 3** shows the normal lung
513 images from Skyscan (**Fig. 3d**), Quantum GX2 (**Fig. 3e**) and nanoScan PET/CT (**Fig.**
514 **3f**) after reconstructing respiratory gated data.
515 **Troubleshooting**
516
517 **Detection of tumours. Timing ~5-15 min per mouse depending on tumour models.**
518 18. Since the signal intensity (HU value) of tumour is similar to lung blood vessel and other
519 soft tissue (both appear grey in images), it is difficult to differentiate between blood
520 vessel and tumours in 2D images. Use the Data viewer software (Skyscan) or Analyze
521 (Quantum GX2) to distinguish the tumours from lung blood vessels.
522 Optional - other widely available 3D viewer software (e.g., ImageJ 3D Viewer.jar,
523 https://imagej.nih.gov/ij/plugins/3d-viewer/)[65]can be used.
524 19. Open the reconstructed data with appropriate 3D viewer.
525 20. Scroll through the image stacks in the Z axis (transverse/axial plane) in respective 3D
526 viewer. We prefer to use the Z axis as a reference plane because it is easier to note
527 down the location of suspicious nodules using the anatomical landmarks. For example,

detection of nodules in right or left lobe of the lung (by using heart), top or bottom of the lung (by using trachea and liver) and near the rib or the spine.

21. Use the crosshairs as visual aids and locate them on the spherical shape which resembles a tumour nodule observed on the Z axis (transverse/axial plane, **Fig. 4a, d**).
22. Simultaneously, check the pattern of the structure on the X (sagittal plane, **Fig. 4b, e**) and Y axes (coronal plane, **Fig. 4c, f**). The blood vessel will appear cylindrical pattern on X and Y axes (**Fig. 4b, c**) and tumours will remain spherical or oval shaped (**Fig. 4e, f**). ▲ **CRITICAL STEP** Once the tumour nodule is detected, record the location of the tumour (as explained in step 20) to monitor the individual tumour volume changes in serial scans.

Individual tumour volume analysis. Timing ~10-30 min depending on tumour models.

23. Tumours with no visible margin (**Fig. 5a**) should be excluded from serial individual tumour volume measurement due to inaccurate tumour segmentation.
24. For accurate tumour segmentation and tracking individual tumour nodules overtime, choose localised tumours without any attachment to surrounding structure and vessel and tumours located near the ribs (Fig. 5b, c), with visible boundaries throughout the slices.
25. For individual tumour development overtime, select the tumours which are identifiable throughout the serial scans for quantification. The same tumours can be identified by comparing the serial scans side by side and in relation to anatomical landmarks (as explained in step 20).
26. Tumour volume analysis can be performed using CTAn software for Skyscan and nanoscan PET/CT data (option A) or Analyze software for Quantum GX2 data (option B)

    (A) CTAn (tumour volume analysis) – Skyscan and nanoscan PET/CT

    i. Load and open the reconstructed dataset (*.bmp; one-bit monochrome or eight-bit grayscale) with CTAn software.
    ii. Optional - change the appearance of the images to colour using a palette bar to enhance the visibility of the tumour (**Fig. 5d**).
    iii. Open ‘Regions of Interest’ tab from main tool bar and draw freehand region of interest (ROI) around tumour and make sure not to include the area which has the same signal intensity as tumour tissue especially near ribs (**Fig. 5e, f**). Some parts of air should be included (**Fig. 5g, h**)

iv. Check ROI throughout the slices and draw and adjust accordingly to include all area of tumour. Typically, the area of tumour is grey, and the surrounding lung tissue is black.

v. Select ‘Empty’ from the ‘Regions of Interest’ tab to empty the ROI on the image when there is no visible tumour to stop the ROIs interpolating.

vi. Save ROI and name the ROI file with the number of tumour and the corresponding Z stack position (e.g., T1-Z422) to prevent confusion in output files.

vii. Reset all ROI and repeat the same procedure (iii-vi). Find all tumours which fulfil above criteria (steps 23-25).

viii. After all tumours are identified, switch to the ‘Binary selection’ tab from the main toolbar.

ix. Set the threshold level for the tumour segmentation by adjusting the binary threshold value to display the tumour area in the ROI as white voxels which are included in the volumetric measurement and the surrounding air/lung area as black voxels which are excluded from the analysis (**Fig. 5i**).

▲ **CRITICAL STEP** In order to ensure unbiased measurements, compare the threshold level between two different datasets from the same animal, for example, before and after the treatment. Set the threshold level which is suitable for all the datasets from different timepoints.

x. Once the threshold is set, create a task list in the custom processing tab using the internal plugins (**Fig. 6a**).

xi. To segment the tumour from the background, start with the plugin called ‘Thresholding’, key in the value from the binary thresholding and then select global (**Fig. 6b**). Black and white image corresponds to the threshold value set will appear after running the plugin (**Fig. 6c-e**).

xii. Select ‘Bitwise operation’ and choose the option: Image = Image and RO to combine image and ROI and generate an image which is the same as the image inside ROI for further processing (**Fig. 6f-h**).

xiii. Optional - To remove all black (space) regions that are fully enclosed by white (solid) voxels select ‘Despeckle’ plugin and choose the option: Remove pores in 2D space by image border and apply to image. This step is useful for removing an abnormal gas-filled region or cavitation within lung nodule (**Fig. 6i-k**).

! Caution

The cavitation can be caused by various aetiologies such as infection, inflammation, and necrosis although it is a rare occurrence in mouse lung

tumour models. There is no standard practice whether to include or exclude the cavitation in the tumour volume measurement. However, the analysis step must be consistent for serial scans.

xiv. Optional - To remove certain white voxels which are not part of tumour, select 'Despeckle' plugin and choose the option: Remove white speckles in 3D space less than 250 voxels (depending on the nature of the lesion) and apply to image.

xv. To calculate the 3D volume measurement, select the '3D analysis' plugin and choose the basic values displayed on the plugin such as total VOI volume, object volume, percent object volume, total VOI surface and object surface.

xvi. Select the value of object volume in mm^3 for the result of the segmented tumour volume.

xvii. Optional - To create a 3D model of the segmented tumours, end the task list with '3D model' plugin and choose the file type: *.ctm and the algorithm: Marching Cubes 33.

xviii. Save the task list and import it for the next dataset.

xix. Optional – CTVol software can be used for 3D volume rendering of individual tumour. It can be useful for demonstrating individual tumour volume changes over time (see an example in anticipated results).

xx. Optional - To perform batch analysis of multiple tumour ROIs from the same dataset, select batch manager icon in custom processing toolbar. Load the dataset and the saved ROI.

! **Caution**

Only one ROI can be applied at a time from the same dataset. Check the name of ROI in output files (see step 26. A (vi) for details) to prevent confusion.

(B) Analyze (tumour volume analysis) – Quantum GX2

i. Load the reconstructed data (*.vox files) on to the analysis program Analyze.

ii. Use Spatial filter under Process tab to improve image quality. Click 'Process', 'Spatial filters' and then select 'Median' and all set to 3 (**Fig. 7a-c**).

iii. To crop the scans and reduce the file size, under Process tab, follow these steps: 'Image calculator', 'Region Pad' and 'Interactive'. Crop the image by clicking on 4 points around the lung image, this will create the yellow box.

Position the box around the lung by dragging the lines so that they are just outside of the rib cage.

iv. Scroll through the image stack to make sure the lung stays within the yellow box. If the lungs move outside the box, adjust the yellow box accordingly. Click Done, then Apply on the Subregion-Pad value, which will now crop the image around the lung (**Fig. 7d-f**). ▲ **CRITICAL STEP** Remember to save the improved image before starting the analysis.

v. Load the images in 'Volume Edit' via 'Segment' tab. To improve the display of the scan, click 'View' tab, select 'Intensities' and then adjust Min/Max range and change the intensity of the image until the contrast between soft tissue and air is clearly defined (**Fig. 7g-i**).

vi. Scroll through the frames on the transverse plane and when a potential tumour is located, click on the tumour and a cross hair will appear allowing to differentiate tumour from pulmonary vessels (see steps 18-22 for details).

vii. For small tumours, it is easier to identify and draw the ROI around the tumour by enlarging the lung image. Right click on lung image, click 'Size' and 'Double' (**Fig. 8a**).

viii. To separate the tumour from the background, click 'Add Object', select 'Wall' tab, tick 'Define Wall', click 'Draw Wall' and then 'Spline' with sensitivity set at 7 (**Extended Data Fig. 1a**).

ix. Draw around the tumour and make sure not to include other areas such as ribs. Some parts of the air can be included.

x. Once the ROI has been drawn around the tumour, right click on the ROI and then click 'Apply' (**Fig. 8b**).

xi. Continue to draw around the tumour every few frames (depending on the size and irregularity of the tumour shape) until the entire tumour from beginning to end is included in the ROI.

xii. Under the 'Semi-Automatic' tab, select 'Region Grow' and click on tumour within drawn line.

xiii. To segment the tumour, adjust the threshold range by changing the Min/Max values either manually or by adjusting the threshold bar **(Extended Data Fig. 1b)**.

xiv. Scroll through the image stack from the beginning to the end of the tumour. The tumour should be completely white (without any black pixels) throughout the image stack, with a clean black outline around the tumour (**Fig. 8c, Extended Data Fig. 1c-e**). Then, click 'Extract Object'.

xv. If the tumour is isolated within the lung, only the tumour area will be highlighted. Scroll through the image on the left and make sure that all part of the tumour is correctly highlighted. Alternatively, click on the tumour image in the right-hand box, hold down Ctrl on the keyboard and observe the tumour at all angles.

xvi. However, if the tumour is attached to background soft tissue or incorrectly drawn around, the whole image will be highlighted (**Fig. 8d, Extended Data Fig. 2a-c**). To correct this, click 'Semi-Automatic' tab and 'Object Separator'. Click on 'Original' in the object window and click anywhere in the lung image other than the tumour (the heart is usually ideal) and then click on the tumour to create two crossed markers. Then click 'Separate' (**Extended Data Fig. 2d**). Scroll through the frames and confirm that the tumour is correctly highlighted.

xvii. If areas outside the tumour have also been highlighted, these can be removed frame by frame by clicking on the 'Manual' tab, select 'Draw' and click on 'Original' on the image window and then erase unwanted highlighted areas using the mouse cursor (**Extended Data Fig. 2e**). Alternatively, erase the sections by moving the cursor over the tumour image on the left-hand side of the screen (**Fig. 8e**).

xviii. Once the whole tumour is highlighted and separated from the rest of the image, click on the box marked 'Locked' (**Extended Data Fig. 2f-h**). This will allow the created ROI to be fixed and separated from the next tumour ROI.

xix. Before drawing the next ROI, under 'Wall' tab, click 'Reset walls' and select 'All'.

xx. Locate next tumour (**Fig. 8f**) and repeat steps vi – xix.

xxi. Once all the tumours have been highlighted, under 'File' tab, click 'Save Object Map' and save in folder with scan data file.

xxii. To calculate the volume of each tumour segmented, go back to the Analyze main window. Click on the data file that you want to analyse. Click on 'Measure' tab and select 'Region of Interest'.

xxiii. Click 'File' on Region of Interest pop-up, select 'Load Object Map' and open the saved tumour object file just created and then click 'Sample Option' tab. Click on 'Objects' in sample type and this should display all the tumours highlighted previously.

xxiv. Set parameters as shown in **Figure 8g** and then click 'Done'. The results will be displayed in a window pop-up and save the file (**Fig. 8h**).

Lung volume analysis. Timing ~10 – 30 min.

27. To indirectly quantify total tumour volume in animal models with widespread diffuse tumour nodules, analyse the lung volume from the end expiration respiratory gated data because it has less motion artefacts and greater image quality.
28. Lung volume analysis can be performed using CTAn software for Skyscan and nanoscan PET/CT data (option A) or Analyze software for Quantum GX2 data (option B)

(A) CTAn (Lung volume analysis) – Skyscan and nanoscan PET/CT

i. Load and open the reconstructed dataset (*.bmp; one-bit monochrome or eight-bit grayscale) with CTAn software.

ii. Optional - change the appearance of the images to colour using a palette bar to enhance the visibility of the lung.

iii. Scroll through the images and identify the start of the airway which situated below the clavicle of the mouse (**Fig. 9a, b**).

iv. Switch to 'Regions of Interest' tab on main toolbar and draw first ROI on the airway (**Fig. 9b**) and set this position as the top of the selection and empty ROI from the below adjacent image.

v. Draw the second ROI on the right lobe of the lung (**Fig. 9c**) and the two ROIs will be interpolated.

vi. Repeat the same procedure throughout the lungs and draw and adjust ROIs accordingly to make sure the whole lung area is included in ROIs (**Fig. 9d, e**).

Troubleshooting

vii. Set the last ROI as the bottom of the selection and empty the ROI from the above adjacent image.

viii. Save the ROI and switch to the 'Binary selection' tab from the main toolbar. To set the threshold level for lung segmentation, adjust the binary threshold value to display the lung/air area in the ROI as white voxels which are included in the volumetric measurement (**Fig. 9f**).

▲ **CRITICAL STEP** For an unbiased measurement, compare the threshold level between two different datasets from the same animal. For example, before the treatment and after the treatment. Set the threshold level which is suitable for all the datasets from different timepoints.

ix. Once the threshold is set, create a task list in custom processing tab.

x. To segment the lung from the background, start with the plugin called 'Thresholding', key in the value from binary thresholding and then select global. Black and white image corresponds to the threshold value set will appear after running the plugin (**Fig. 9g-i**).

xi. Select 'Bitwise operation' and choose the option: Image = Image and ROI to combine image and ROI and generate an image which is the same as the image inside ROI for further processing (**Fig. 9j-l**).

Optional – Noise and image artefacts may appear as white speckles, remove them by selecting the 'Despeckle' plugin and choose the option: Remove white speckles in 3D space less than 200 voxels (depending on the nature of the artefacts and radiological pattern) and apply it to image. For example, in a doxycycline inducible autochthonous mouse model of epidermal growth factor receptor $(EGFR)^{L858R}$ -driven lung cancer, the diffuse pattern of air distribution needs to be finely adjusted using the 'Despeckle' plugin (**Fig. 9m-o**).

xii. To calculate the 3D volumes, select the '3D analysis' plugin and choose basic values displayed on the plugin such as total VOI volume, object volume, percent object volume, total VOI surface and object surface.

xiii. Select the value of object volume in mm^3 for the result of the segmented lung/air volume.

xiv. Optional - To create a 3D model of the segmented lung volume, end the task list with '3D model' plugin and choose the file type: *.ctm and algorithm: Marching Cubes 33.

xv. Save the task list and import it again for the next dataset.

xvi. Optional – CTVol software can be used for 3D volume rendering of segmented lung.

(B) Analyze (Lung volume analysis) – Quantum GX2

i. Repeat the steps i – v from Analyze (tumour volume analysis). To perform the automatic segmentation of lung from the background, the signal intensity of trachea (for air) and heart (for tissue including blood, water, cells) will be used as calibrators.

ii. Scroll through the beginning of the image stack until the trachea is observed (**Fig. 10a**).

iii. Under the 'Semi-Automatic' tab, select 'Region Grow', click on the middle of the trachea, and adjust the 'Threshold' to display the trachea as white

voxels and the background tissue as black voxels **(Fig. 10b, Extended Data Fig. 3a-d)**.

iv. Click ‘Extract Object’. Not all parts of trachea need to be thresholded and highlighted when it appears in the 3D volume rendering window (**Fig. 10c**).

v. Click ‘Add Object’, under ‘Manual’ tab, select ‘Draw’ and highlight two points in the heart by clicking and scrolling through the frames, and clicking again (**Fig. 10d, e, Extended Data Fig. 3e**).

vi. Under ‘Semi-Automatic’ tab, select ‘Propagate Object’ and ‘Propagate’. ▲ **CRITICAL STEP** Make sure the new object observed is cylindrical (**Fig. 10f**).

vii. Save the object map in ‘File’ tab as ‘calibration’.

viii. To calculate the mean signal intensity of the trachea and heart, go back to the Analyze main window and click on the data you want to analyse.

ix. Select ‘Region of Interest’ under ‘Measure’ tab.

x. Select ‘File’ on region of interest pop-up, click ‘Load Object Map’ and open the saved ‘calibration’ object file just created.

xi. Click the ‘Sample Option’ tab and select ‘Objects’ in the sample type and the two structures (trachea and heart) highlighted previously will appear.

xii. Set the parameters as shown in **Extended Data Fig. 4a** and then click ‘Done’. The results will be displayed in a window pop-up.

xiii. Save the file.

xiv. Create a linear HU calibration curve and equation as shown in **Extended Data Fig. 4b** using the mean signal intensity of trachea (-1000 HU) and heart (0 HU) from the results.

xv. To perform the segmentation of the lung, go back to the Analyze main window and click on the data you want to analyse.

xvi. Click the ‘Process’ tab and select ‘Image Algebra’ (**Extended Data Fig. 4c**).

xvii. Drag the data from the Analyze window to image in ‘Input’ and then click on ‘Output’. On ‘Name’ tab, click on the image ID and then add an underscore (_) to the end of the ID (**Extended Data Fig. 4d**).

xviii. Set ‘Data type’ to ‘Signed 16-bit’.

xix. Click ‘Done’ (**Extended Data Fig. 4d**).

xx. In the formula section of Image Alegra, fill in this equation: Output = (Input - 2nd Y value)/1st Y value and then click ‘Go’ (**Extended Data Fig. 4d**). This should create a new lung image in the Analyze window.

xxi. Click on the image and save the file.

xxii. Load the new lung image in ‘Volume Edit’ via ‘Segment’ tab. Under the ‘Semi-Automatic’ tab, select ‘Region grow’ and click on anywhere in the lung image that is air.

xxiii. Set Min threshold to absolute minimum and Max to -300 (**Fig. 10g, Extended Data Fig. 4e**).

xxiv. Click ‘Extract Object’ and the highlighted lung should appear in the volume rendering panel. Hold Ctrl key on keyboard and rotate the image with the mouse cursor to verify that the whole lung has been correctly highlighted. Alternatively, right click on the image and select ‘Reset rotation’ to observe at various angles (**Fig. 10h, i**).

xxv. Save the Object map by clicking on ‘File’ tab.

xxvi. To calculate the volume of the segmented lung, go back to the Analyze main window. Click on the lung image you want to analyse. Under the ‘Measure’ tab, click on ‘Region of Interest’ and select ‘file’ on the region of interest pop-up.

xxvii. Click ‘Load Object Map’ and open the saved whole lung object file just created.

xxviii. Under ‘Sample Option’ tab, click on ‘Objects’ in the sample type and this should display the segmented lung dataset.

xxix. Set parameters as shown in **Figure 10j** and click ‘Done’. The results will be displayed in a window pop-up.

xxx. Save the file (**Fig. 10k**).

xxxi. To determine absolute air volume (i.e., removal of infiltrate etc), open an excel sheet and create the equations (see below) using the mean HU and the volume (mm^3) of whole lung from the results.

%change = Mean HU*- 0.001

Actual lung volume = Vol_mm3*%change

xxxii. Calculate the percentage of air and tissue as shown in **Figure 10l**.

Troubleshooting

Troubleshooting advice can be found in Table 3.

Timing

The time required for each step depending on the experience of the user. The first-time users may require more time for each step.

Steps 1-10, animal preparation: 5-8 min

Steps 11-15, image acquisition: 5-10 min

Steps 16-17, respiratory gating, and reconstruction: 3-5 min
Steps 18-22, detection of tumours: 5-15 min depending on tumour models
Steps 23-26, individual tumour volume analysis: 10-30 min depending on tumour models
Steps 27-28, lung volume analysis: 10-30 min

Anticipated results

This protocol will enable the researchers to acquire high-resolution images (see table 1 for the resolution of each scanner) of lung tumours and allows to characterise radiological phenotypes of each model, monitor tumour progression, track individual tumour nodules, identify lung volume transformation, and evaluate therapeutic response. In order to differentiate very small tumour nodules from the vessels accurately, we recommend starting the analysis after two or more serial scans to track the changes in suspicious areas, for example, the tumour will appear bigger whereas the blood vessels will remain the same (**Fig. 11a-f**). Although creating representative 3D images of analysed tumours and lungs is an optional step, it is very useful in visualising contrasting therapeutic response in the same animal over time. For example, in the KRAS-driven lung tumour model, increases, decreases and no change of individual tumour volume after treating with mitogen-activated protein kinase kinase (MEK) inhibitor can be detected very clearly using 3D models (**Fig. 11g-i**). Based on our experience with this protocol, we anticipate any researcher with a basic scientific skillset will be able to perform image acquisition independently after 5-8 animals. Image analysis, however, likely requires more practice (up to 20 animals per model) to be able to execute the steps efficiently.

Acknowledgements

We would like to dedicate this work to Francois Lassailly who was instrumental in setting up the *In Vivo* Imaging Facility at the Francis Crick Institute. We thank Dr Elza de Bruin (AstraZeneca) for providing images from EGFR mutation model. We thank Nicholas Corps (Skyscan, Bruker), Sasha Belenkov and Jack Sharkey (PerkinElmer) and Miklos Kovacs (Mediso) for providing technical assistance with the respective scanners and software. We thank the Francis Crick Institute Biological Research facilities for technical assistance. This work was supported by the Francis Crick Institute, which receives its core funding from Cancer Research UK (FC001039), the UK Medical Research Council (FC001039) and the Wellcome Trust (FC001039).

Author contributions

M.Z.T., developed and tested the protocol in PET/CT scanner. M.Z.T., C.M., and T.S., developed and tested the protocol in two micro-CT scanners. M.Z.T., C.M., and T.S., acquired

and analysed the data. M.Z.T. wrote the manuscript and C.M., and T.S., provided technical details. T.K., A.B., and J.D. supervised the study. All authors edited the manuscript and approved the final version.

Competing interests

J.D. has acted as a consultant for AstraZeneca, Jubilant, Theras, BridgeBio and Vividion, and has funded research agreements with BMS and Revolution Medicines. None of the other authors of this manuscript have a financial interest related to this work.

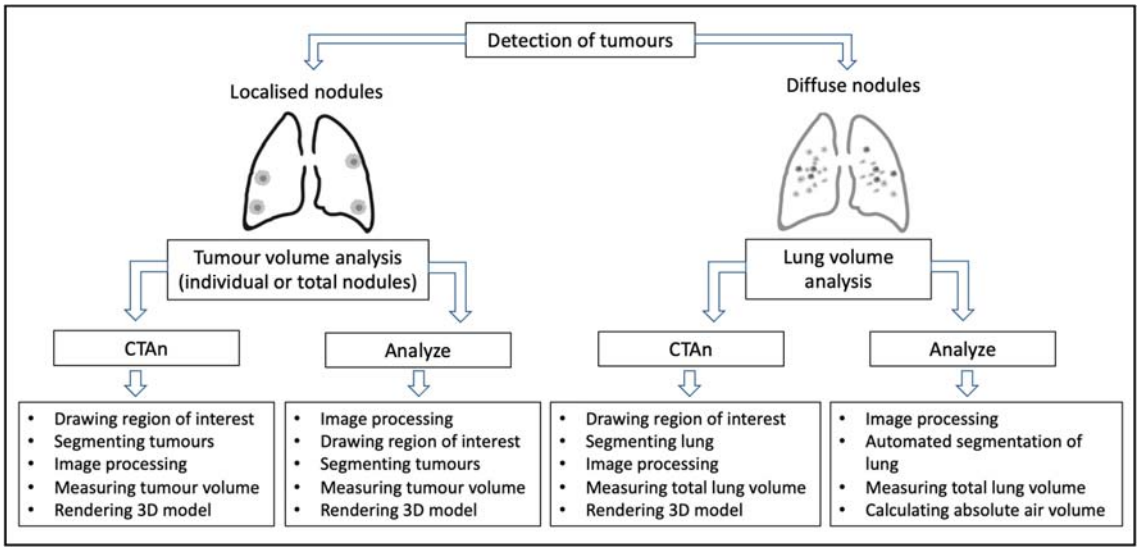

Box 1. Summary of the analysis pipeline for lung tumour quantification.

Table 1 Imaging parameters used in the study for respiratory gated lung scans. Individual imaging parameters should be optimised depending on the micro-CT scanner.

	Skyscan 1176	Quantum GX2	nanoScan PET/CT
X-ray source kilovolt peak (kVp)	50	90	50
X-ray source current (uA)	500	88	670

Exposure time (ms)	60	16.67	300
Field of view (mm)	35	36	52 (medium zoom)
Filter (mm)	Al 0.5	Cu 0.06+Al 0.5	Al 1.8
Scan mode	List mode (8)	High speed (Resp Gated)	Semicircular
Scanning duration (min)	8	4	3.5
Resolution (μm)	35 (pixel size)	50 (voxel size)	65 (1:4 binning, voxel size)
Radiation dose (mGy)	1362.4 (170.3 mGy/min)[a]	926.5[b]	219[c]

914 [a]Using SpekCalc[66-68]
915 [b]CT dose index 100 ($CTDI_{100}$, ionisation chamber)[69]
916 [c]CT dose index (CTDI)
917

918 **Table 2** Example of reconstruction parameters for the respiratory gated lung scan. Individual
919 parameters should be optimised depending on the micro-CT scanner.

	Skyscan	Quantum GX2	nanoScan PET/CT
Retrospective Respiratory gating	RespGate (End expiration)	End expiration	RespGate (End expiration)
Reconstruction software	NRecon	Integrated in Quantum GX2 4.0 control software	Nucline
Reconstruction parameter	Smoothing: 4 Beam hardening: 30%	Ring artefact reduction and beam hardening correction enabled	Medium slice thickness, medium in-plane voxel Butterworth filter

920

921 **Table 3** Troubleshooting table

Step	Problem	Possible Reason	Solution
3	Mouse breathing increases when it is transferred to the bed	Movement of mouse causes breathing irregularities.	Increase O2 flow rate to 1L/min or the percentage of isoflurane to 3% and return it back to 2% once the breathing is stable.
10	Mouse having erratic breathing	High tumour burden in the lung	Allow the mouse to fully recover from the

			anaesthesia and then anaesthetise again.
11	Part of the lung image is cut out of the scan	Bed is too close to the X-ray source	Rotate the CT gantry to 180 degrees around the mouse and check on the video display if all parts of the lung stay with the FOV. If not, adjust the position of the bed and repeat the same step.
17	Blurry image	Problem with scanner alignment	Perform alignment or geometric calibration
28. A (vi)	Unrepresentative structures in 3D lung volume rendering (CTAn, Extended Data Fig. 5a)	Incorporation of fat (Extended Data Fig. 5b), gas shadow from stomach (Extended Data Fig. 5c), motion artefact from the ribs (Extended Data Fig. 5d) and the spine in ROI of lung (Extended Data Fig. 5e)	Re-draw or edit the ROI of lung

Figure legends:

Figure 1. Common radiological characteristics of lung tumour models. a-c) KRAS-driven multiple lung tumour nodules with (b) smooth and (c) spiculated margins. d) Lobulated lung nodules in urethane-induced model. e) Lung nodules with well-defined margin in orthotopic intratracheal model. f-i) $EGFR^{L858R}$-mutant lung tumours with (f) widespread diffuse nodules, (g) a mixture of (h) ground-glass appearances and (i) discrete lesions. j) Diffused pattern of lung tumours in tail vein cell injection model.

Figure 2. Summary of the workflow for the lung tumour imaging with micro-CT and tumour volume analysis.

Figure 3. Micro-CT acquisition. a) The anesthetised mouse is inserted inside the nose cone on the bed. b) The front paws of the mouse should be gently taped down to have a clear view of the thorax. c) Video image pop-up screen of the mouse in the Quantum GX2 scanner, with the blue square indicating the field of view for the scan and the green rectangle (arrow) placed

partially over the diaphragm for respiratory gating. d-f) Reconstructed normal lung images of different mice from (d) Skyscan, (e) Quantum GX2 & (f) nanoScan PET/CT.

Figure 4. Differentiation of tumours from normal structure in 3D. a-c) Blood vessel centred with crosshairs appears (a) spherical shape in axial plane (Z axis, blue line) and cylindrical in (b) sagittal plane (X axis, red line) & (c) coronal plane (Y axis, green line). d-f) Lung tumour appears spherical shape in all axes (crosshairs) from the same animal.

Figure 5. Individual tumour nodule segmentation using CTAn software. a-c) Lung tumour with (a) no visible margins (black arrow), tumours with no attachment to surrounding structures (blue arrows) and (b-c) located near ribs (red arrows). d) A small tumour nodule locating near spine (blue arrows) in enhanced colour display. e-h) Images of freehand ROI drawing on tumours showing (e, g) before & (f, h) after ROI selections which exclude signal from the rib and include some regions of air. i) Tumour segmentation using binary threshold adjustment under binary selection tab to transform the area within ROI into white voxels for volumetric measurement and the green area indicates outside the ROI. All the images are from *Kras* mutant lung tumour model.

Figure 6. Individual tumour volume measurements using CTAn software. a) List of the internal plugins under the custom processing tab. b) Pop-up window showing selected parameters for thresholding. c-e) Binary thresholded images before bitwise plugin showing (c) image view of the whole lung with (inset) tumour, (d, inset) image inside ROI view & (e, inset) ROI view of segmented tumour from the background. f-h) Binary thresholded images of segmented tumour after bitwise plugin creating (f, inset) the image which is the same as (g, inset) the image inside ROI but leaving (h, inset) ROI view unchanged. i-k) Tumour with gas-filled area (blue arrows) showing (i) ROI selection, (j) black and white image of ROI selection under binary selection tab and (k) the black area inside the segmented tumour being removed by the despeckle plugin.

Figure 7. Improving image quality with Analyze software. a) Image showing main command window of Analyze. b) Screenshot of the pop-up window of the Spatial filter and the selected parameters for the filter set. c-d) Data processing steps to crop the scan using (c) Image calculator & region pad tool followed by (d) interactive window selection. e-f) Lung images showing (e) before & (f) after cropping. g-i) Images showing how to achieve (g) lung images with a well-defined contrast between air, soft tissue and tumour (centred with crosshairs) by adjusting the signal intensity of the image via selecting (h) the intensities tab and (i) adjusting the minimum and maximum values tool under the ‘Volume Edit’ command window.

Figure 8. Individual tumour segmentation and quantification using Analyze software. a-c) Axial images showing step by step identification and highlighting of tumour starting with (a) enlarging image to identify the tumours in the lung followed by (b) highlighting tumour using drawing a wall and (c) adjusting the binary threshold range to segment and extract the tumour from the background. d-f) Axial images showing how to (d) separate the tumour from surrounding tissue when it is attached to the background, (e) remove any additional tissue attachments using manual deletion tool and (f) lock previous tumour selection and reset wall before highlighting new tumour for segmentation. g-h) Images showing step by step analysis of tumour volume quantification by (g) setting parameters for tumour analysis and (h) generating tumour volume measurement.

Figure 9. Lung volume segmentation using the CTAn software. a) Preview image of Z-stack showing the start of the airway below the clavicle (black line). b-e) Drawing ROI on (b) the start of the airway, (c) the right lobe, (d) the start of the left lobe and (e) the whole lung. f) Lung segmentation using binary thresholding to transform the area within ROI into white voxels for volumetric measurement. g-i) Binary thresholded images before bitwise plugin showing (g) image view of the whole lung, (h) image inside ROI view & (i) ROI view of segmented lung from the background. j-l) Binary thresholded images of segmented lung after bitwise plugin creating (j) the image which is the same as (k) the image inside ROI but leaving (l) ROI view unchanged. m-o) Lung images from *EGFR*^{L858R} mutant model showing (m) ROI selected diffuse air pattern with artefacts from the spine, (n) thresholded image before & (o) after despeckle plugin removing white speckles image artefacts (blue dotted box). All the images are from the same mouse with *EGFR*^{L858R} mutation.

Figure 10. Automatic lung segmentation and volume quantification with Analyze software. a-c) Images showing step by step identification and highlighting of trachea starting with (a) localisation of trachea, (b) inputting threshold for trachea and (c) 3D volume rendered image of extracted trachea. d-f) Images showing the highlighted regions of the heart (d) in axial (green dot) & (e) 3D volume rendered (green line) images by using the tool called ‘Draw’ and then (f) joining the highlighted sections via propagation as presented in 3D volume rendered image. g) Binary thresholded image of lung after calculating signal intensity of air inside the lung. h-i) Images showing (h) the segmented lung from the background after setting threshold values, and (i) how to inspect the segmented 3D lung image by right clicking on image and using rotation angle. j-l) Images showing lung volume analysis by (j) setting parameters for quantification, (k) generating the results and (l) acquiring absolute air volume in the lung using equation as shown in excel.

1013

1014 Figure 11 Tracking individual tumour volume changes over time. a-f) Serial CT lung images
1015 from *Kras* mutant lung tumour model showing volumetric changes in tumour nodules (red
1016 arrows) and no alteration (blue arrows) detected in blood vessel. g-i) Serial 3D rendered
1017 images of *Kras* mutant lung tumours showing decrease (yellow), increase (magenta), and no
1018 changes (green) in tumour volume (g) before, (h) 1 week & (i) 2 weeks after treating with MEK
1019 inhibitor. All 3D models were generated with Bruker's CT vol software.

1020

1021

1022

1023 **References**

1024 1 Sung, H. *et al.* Global Cancer Statistics 2020: GLOBOCAN Estimates of Incidence and
1025 Mortality Worldwide for 36 Cancers in 185 Countries. *CA: A Cancer Journal for*
1026 *Clinicians* **71**, 209-249, doi:https://doi.org/10.3322/caac.21660 (2021).
1027 2 Graham, M. L. & Prescott, M. J. The multifactorial role of the 3Rs in shifting the
1028 harm-benefit analysis in animal models of disease. *Eur J Pharmacol* **759**, 19-29,
1029 doi:10.1016/j.ejphar.2015.03.040 (2015).
1030 3 Hounsfield, G. N. Computed medical imaging. Nobel lecture, Decemberr 8, 1979. *J*
1031 *Comput Assist Tomogr* **4**, 665-674, doi:10.1097/00004728-198010000-00017 (1980).
1032 4 Lev, M. H. & Gonzalez, R. G. in *Brain Mapping: The Methods (Second Edition)* (eds
1033 Arthur W. Toga & John C. Mazziotta) 427-484 (Academic Press, 2002).
1034 5 Bibb, R., Eggbeer, D. & Paterson, A. in *Medical Modelling (Second Edition)* (eds
1035 Richard Bibb, Dominic Eggbeer, & Abby Paterson) 7-34 (Woodhead Publishing,
1036 2015).
1037 6 Jonas, D. E. *et al.* Screening for Lung Cancer With Low-Dose Computed Tomography:
1038 Updated Evidence Report and Systematic Review for the US Preventive Services Task
1039 Force. *JAMA* **325**, 971-987, doi:10.1001/jama.2021.0377 (2021).
1040 7 Castellano, E. *et al.* Requirement for interaction of PI3-kinase p110α with RAS in lung
1041 tumor maintenance. *Cancer Cell* **24**, 617-630, doi:10.1016/j.ccr.2013.09.012 (2013).
1042 8 de Bruin, E. C. *et al.* Reduced NF1 expression confers resistance to EGFR inhibition in
1043 lung cancer. *Cancer Discov* **4**, 606-619, doi:10.1158/2159-8290.Cd-13-0741 (2014).
1044 9 Molina-Arcas, M. *et al.* Development of combination therapies to maximize the
1045 impact of KRAS-G12C inhibitors in lung cancer. *Science translational medicine* **11**,
1046 doi:10.1126/scitranslmed.aaw7999 (2019).
1047 10 Spiro, J. E. *et al.* Monitoring treatment effects in lung cancer-bearing mice: clinical CT
1048 and clinical MRI compared to micro-CT. *European Radiology Experimental* **4**, 31,
1049 doi:10.1186/s41747-020-00160-7 (2020).
1050 11 Rudyanto, R. D. *et al.* Individual nodule tracking in micro-CT images of a longitudinal
1051 lung cancer mouse model. *Medical Image Analysis* **17**, 1095-1105,
1052 doi:https://doi.org/10.1016/j.media.2013.07.002 (2013).
1053 12 Holdsworth, D. W. & Thornton, M. M. Micro-CT in small animal and specimen
1054 imaging. *Trends in Biotechnology* **20**, S34-S39, doi:https://doi.org/10.1016/S0167-
1055 7799(02)02004-8 (2002).

1056 13 Clark, D. P. & Badea, C. T. Micro-CT of rodents: state-of-the-art and future
1057 perspectives. *Phys Med* **30**, 619-634, doi:10.1016/j.ejmp.2014.05.011 (2014).
1058 14 Ford, N. L., Wheatley, A. R., Holdsworth, D. W. & Drangova, M. Optimization of a
1059 retrospective technique for respiratory-gated high speed micro-CT of free-breathing
1060 rodents. *Phys Med Biol* **52**, 5749-5769, doi:10.1088/0031-9155/52/19/002 (2007).
1061 15 Ertel, D., Kyriakou, Y., Lapp, R. M. & Kalender, W. A. Respiratory phase-correlated
1062 micro-CT imaging of free-breathing rodents. *Phys Med Biol* **54**, 3837-3846,
1063 doi:10.1088/0031-9155/54/12/015 (2009).
1064 16 Kumar, M. S. *et al.* The GATA2 transcriptional network is requisite for RAS oncogene-
1065 driven non-small cell lung cancer. *Cell* **149**, 642-655, doi:10.1016/j.cell.2012.02.059
1066 (2012).
1067 17 Foster, H. *et al.* ATMIN Is a Tumor Suppressor Gene in Lung Adenocarcinoma. *Cancer*
1068 *Res* **79**, 5159-5166, doi:10.1158/0008-5472.Can-19-0647 (2019).
1069 18 de Carné Trécesson, S. *et al.* APOBEC3B expression generates an immunogenic
1070 model of Kras mutant lung cancer. *bioRxiv*, 2020.2012.2022.423126,
1071 doi:10.1101/2020.12.22.423126 (2020).
1072 19 Kennel, S. J. *et al.* High resolution computed tomography and MRI for monitoring
1073 lung tumor growth in mice undergoing radioimmunotherapy: correlation with
1074 histology. *Med Phys* **27**, 1101-1107, doi:10.1118/1.598974 (2000).
1075 20 Fushiki, H. *et al.* Quantification of mouse pulmonary cancer models by
1076 microcomputed tomography imaging. *Cancer Sci* **100**, 1544-1549,
1077 doi:10.1111/j.1349-7006.2009.01199.x (2009).
1078 21 van Maldegem, F. *et al.* Characterisation of tumour microenvironment remodelling
1079 following oncogene inhibition in preclinical studies with imaging mass cytometry.
1080 *Nature Communications* **12**, 5906, doi:10.1038/s41467-021-26214-x (2021).
1081 22 Vande Velde, G. *et al.* Longitudinal micro-CT provides biomarkers of lung disease
1082 that can be used to assess the effect of therapy in preclinical mouse models, and
1083 reveal compensatory changes in lung volume. *Dis Model Mech* **9**, 91-98,
1084 doi:10.1242/dmm.020321 (2016).
1085 23 Marien, E., Hillen, A., Vanderhoydonc, F., Swinnen, J. V. & Vande Velde, G.
1086 Longitudinal microcomputed tomography-derived biomarkers for lung metastasis
1087 detection in a syngeneic mouse model: added value to bioluminescence imaging.
1088 *Laboratory Investigation* **97**, 24-33, doi:10.1038/labinvest.2016.114 (2017).
1089 24 DuPage, M., Dooley, A. L. & Jacks, T. Conditional mouse lung cancer models using
1090 adenoviral or lentiviral delivery of Cre recombinase. *Nature Protocols* **4**, 1064-1072,
1091 doi:10.1038/nprot.2009.95 (2009).
1092 25 Westcott, P. M. *et al.* The mutational landscapes of genetic and chemical models of
1093 Kras-driven lung cancer. *Nature* **517**, 489-492, doi:10.1038/nature13898 (2015).
1094 26 Politi, K., Fan, P. D., Shen, R., Zakowski, M. & Varmus, H. Erlotinib resistance in
1095 mouse models of epidermal growth factor receptor-induced lung adenocarcinoma.
1096 *Dis Model Mech* **3**, 111-119, doi:10.1242/dmm.003681 (2010).
1097 27 Politi, K. *et al.* Lung adenocarcinomas induced in mice by mutant EGF receptors
1098 found in human lung cancers respond to a tyrosine kinase inhibitor or to down-
1099 regulation of the receptors. *Genes Dev* **20**, 1496-1510, doi:10.1101/gad.1417406
1100 (2006).

1101 28 Bianchi, A. *et al.* In vivo MRI for effective non-invasive detection and follow-up of an
1102 orthotopic mouse model of lung cancer. *NMR Biomed* **27**, 971-979,
1103 doi:10.1002/nbm.3142 (2014).
1104 29 Krupnick, A. S. *et al.* Quantitative monitoring of mouse lung tumors by magnetic
1105 resonance imaging. *Nat Protoc* **7**, 128-142, doi:10.1038/nprot.2011.424 (2012).
1106 30 Neijenhuis, L. K. A. *et al.* Near-Infrared Fluorescence Tumor-Targeted Imaging in
1107 Lung Cancer: A Systematic Review. *Life (Basel)* **12**, doi:10.3390/life12030446 (2022).
1108 31 Imamura, T., Saitou, T. & Kawakami, R. In vivo optical imaging of cancer cell function
1109 and tumor microenvironment. *Cancer Science* **109**, 912-918,
1110 doi:https://doi.org/10.1111/cas.13544 (2018).
1111 32 Christensen, J., Vonwil, D. & Shastri, V. P. Non-Invasive In Vivo Imaging and
1112 Quantification of Tumor Growth and Metastasis in Rats Using Cells Expressing Far-
1113 Red Fluorescence Protein. *PLoS One* **10**, e0132725,
1114 doi:10.1371/journal.pone.0132725 (2015).
1115 33 Kocher, B. & Piwnica-Worms, D. Illuminating cancer systems with genetically
1116 engineered mouse models and coupled luciferase reporters in vivo. *Cancer Discov* **3**,
1117 616-629, doi:10.1158/2159-8290.Cd-12-0503 (2013).
1118 34 Ju, H.-L. *et al.* Transgenic mouse model expressing P53R172H, luciferase, EGFP and
1119 KRASG12D in a single open reading frame for live imaging of tumor. *Scientific reports*
1120 **5**, 8053, doi:10.1038/srep08053 (2015).
1121 35 Yeh, H. H. *et al.* Molecular imaging of active mutant L858R EGF receptor (EGFR)
1122 kinase-expressing nonsmall cell lung carcinomas using PET/CT. *Proc Natl Acad Sci U S*
1123 *A* **108**, 1603-1608, doi:10.1073/pnas.1010744108 (2011).
1124 36 Price, D. N. *et al.* Longitudinal Assessment of Lung Cancer Progression in Mice Using
1125 the Sodium Iodide Symporter Reporter Gene and SPECT/CT Imaging. *PLOS ONE* **11**,
1126 e0169107, doi:10.1371/journal.pone.0169107 (2016).
1127 37 Marsee, D. K. *et al.* Imaging of metastatic pulmonary tumors following NIS gene
1128 transfer using single photon emission computed tomography. *Cancer Gene Therapy*
1129 **11**, 121-127, doi:10.1038/sj.cgt.7700661 (2004).
1130 38 Nielsen, C. H. *et al.* PET imaging of tumor neovascularization in a transgenic mouse
1131 model with a novel 64Cu-DOTA-knottin peptide. *Cancer Res* **70**, 9022-9030,
1132 doi:10.1158/0008-5472.Can-10-1338 (2010).
1133 39 Umeda, I. O. *et al.* High resolution SPECT imaging for visualization of intratumoral
1134 heterogeneity using a SPECT/CT scanner dedicated for small animal imaging. *Annals*
1135 *of Nuclear Medicine* **26**, 67-76, doi:10.1007/s12149-011-0542-7 (2012).
1136 40 Khalil, M. M., Tremoleda, J. L., Bayomy, T. B. & Gsell, W. Molecular SPECT Imaging:
1137 An Overview. *International Journal of Molecular Imaging* **2011**, 796025,
1138 doi:10.1155/2011/796025 (2011).
1139 41 Hekman, M. C. H. *et al.* Detection of Micrometastases Using SPECT/Fluorescence
1140 Dual-Modality Imaging in a CEA-Expressing Tumor Model. *J Nucl Med* **58**, 706-710,
1141 doi:10.2967/jnumed.116.185470 (2017).
1142 42 Zhang, Y. *et al.* Preliminary application of micro-SPECT/CT imaging by 99mTc-tricine-
1143 EDDA-HYNIC-c-Met for non-small-cell lung cancer. *Chemical Biology & Drug Design*
1144 **93**, 447-453, doi:https://doi.org/10.1111/cbdd.13432 (2019).
1145 43 Versagli, C. *et al.* Multimodal Optical, X-ray CT, and SPECT Imaging of a Mouse Model
1146 of Breast Cancer Lung Metastasis. *Current molecular medicine* **13**,
1147 doi:10.2174/1566524011313030006 (2013).

1148 44 V, G. *et al.* Development of novel approach to diagnostic imaging of lung cancer with
1149 18F-Nifene PET/CT using A/J Mice treated with NNK. *Journal of Cancer Research and*
1150 *Therapy* **1**, 128-137, doi:10.14312/2052-4994.2013-20 (2013).
1151 45 Puaux, A.-L. *et al.* A Comparison of Imaging Techniques to Monitor Tumor Growth
1152 and Cancer Progression in Living Animals. *International Journal of Molecular Imaging*
1153 **2011**, 321538, doi:10.1155/2011/321538 (2011).
1154 46 Yang, Z. *et al.* Dynamic FDG-PET Imaging to Differentiate Malignancies from
1155 Inflammation in Subcutaneous and In Situ Mouse Model for Non-Small Cell Lung
1156 Carcinoma (NSCLC). *PLOS ONE* **10**, e0139089, doi:10.1371/journal.pone.0139089
1157 (2015).
1158 47 Molinos, C. *et al.* Low-Dose Imaging in a New Preclinical Total-Body PET/CT Scanner.
1159 *Frontiers in Medicine* **6**, doi:10.3389/fmed.2019.00088 (2019).
1160 48 Plathow, C. *et al.* Computed Tomography Monitoring of Radiation-Induced Lung
1161 Fibrosis in Mice. *Investigative Radiology* **39**, 600-609,
1162 doi:10.1097/01.rli.0000138134.89050.a5 (2004).
1163 49 Berghen, N. *et al.* Radiosafe micro-computed tomography for longitudinal evaluation
1164 of murine disease models. *Scientific reports* **9**, 17598, doi:10.1038/s41598-019-
1165 53876-x (2019).
1166 50 Detombe, S. A., Dunmore-Buyze, J., Petrov, I. E. & Drangova, M. X-ray dose delivered
1167 during a longitudinal micro-CT study has no adverse effect on cardiac and pulmonary
1168 tissue in C57BL/6 mice. *Acta Radiol* **54**, 435-441, doi:10.1177/0284185113475608
1169 (2013).
1170 51 Vande Velde, G. *et al.* Longitudinal in vivo microcomputed tomography of mouse
1171 lungs: No evidence for radiotoxicity. *Am J Physiol Lung Cell Mol Physiol* **309**, L271-
1172 279, doi:10.1152/ajplung.00098.2015 (2015).
1173 52 Li, J. *et al.* A novel functional CT contrast agent for molecular imaging of cancer. *Phys*
1174 *Med Biol* **55**, 4389-4397, doi:10.1088/0031-9155/55/15/013 (2010).
1175 53 Gómez-López, S., Whiteman, Z. E. & Janes, S. M. Mapping lung squamous cell
1176 carcinoma pathogenesis through in vitro and in vivo models. *Communications*
1177 *Biology* **4**, 937, doi:10.1038/s42003-021-02470-x (2021).
1178 54 You, M. S., Rouggly, L. C., You, M. & Wang, Y. Mouse models of lung squamous cell
1179 carcinomas. *Cancer and Metastasis Reviews* **32**, 77-82, doi:10.1007/s10555-012-
1180 9406-4 (2013).
1181 55 Singh, A. P., Adrianzen Herrera, D., Zhang, Y., Perez-Soler, R. & Cheng, H. Mouse
1182 models in squamous cell lung cancer: impact for drug discovery. *Expert Opinion on*
1183 *Drug Discovery* **13**, 347-358, doi:10.1080/17460441.2018.1437137 (2018).
1184 56 Ruiz, E. J. *et al.* LUBAC determines chemotherapy resistance in squamous cell lung
1185 cancer. *Journal of Experimental Medicine* **216**, 450-465, doi:10.1084/jem.20180742
1186 (2019).
1187 57 Montgomery, M. K. *et al.* Mouse lung automated segmentation tool for quantifying
1188 lung tumors after micro-computed tomography. *PLoS One* **16**, e0252950,
1189 doi:10.1371/journal.pone.0252950 (2021).
1190 58 Birk, G., Kästle, M., Tilp, C., Stierstorfer, B. & Klee, S. Automatization and
1191 improvement of µCT analysis for murine lung disease models using a deep learning
1192 approach. *Respir Res* **21**, 124, doi:10.1186/s12931-020-01370-8 (2020).

1193 59 Haines, B. B. *et al.* A quantitative volumetric micro-computed tomography method
1194 to analyze lung tumors in genetically engineered mouse models. *Neoplasia* **11**, 39-
1195 47, doi:10.1593/neo.81030 (2009).
1196 60 Gallastegui, A., Cheung, J., Southard, T. & Hume, K. R. Volumetric and linear
1197 measurements of lung tumor burden from non-gated micro-CT imaging correlate
1198 with histological analysis in a genetically engineered mouse model of non-small cell
1199 lung cancer. *Lab Anim* **52**, 457-469, doi:10.1177/0023677218756457 (2018).
1200 61 Workman, P. *et al.* Guidelines for the welfare and use of animals in cancer research.
1201 *Br J Cancer* **102**, 1555-1577, doi:10.1038/sj.bjc.6605642 (2010).
1202 62 Jackson, E. L. *et al.* The differential effects of mutant p53 alleles on advanced murine
1203 lung cancer. *Cancer Res* **65**, 10280-10288, doi:10.1158/0008-5472.Can-05-2193
1204 (2005).
1205 63 DuPage, M., Dooley, A. L. & Jacks, T. Conditional mouse lung cancer models using
1206 adenoviral or lentiviral delivery of Cre recombinase. *Nat Protoc* **4**, 1064-1072,
1207 doi:10.1038/nprot.2009.95 (2009).
1208 64 Farncombe, T. H. Software-based respiratory gating for small animal conebeam CT.
1209 *Med Phys* **35**, 1785-1792, doi:10.1118/1.2905031 (2008).
1210 65 Schneider, C. A., Rasband, W. S. & Eliceiri, K. W. NIH Image to ImageJ: 25 years of
1211 image analysis. *Nat Methods* **9**, 671-675, doi:10.1038/nmeth.2089 (2012).
1212 66 Poludniowski, G., Landry, G., DeBlois, F., Evans, P. M. & Verhaegen, F. SpekCalc: a
1213 program to calculate photon spectra from tungsten anode x-ray tubes. *Physics in*
1214 *Medicine and Biology* **54**, N433-N438, doi:10.1088/0031-9155/54/19/n01 (2009).
1215 67 Poludniowski, G. G. & Evans, P. M. Calculation of x-ray spectra emerging from an x-
1216 ray tube. Part I. Electron penetration characteristics in x-ray targets. *Medical Physics*
1217 **34**, 2164-2174, doi:https://doi.org/10.1118/1.2734725 (2007).
1218 68 Poludniowski, G. G. Calculation of x-ray spectra emerging from an x-ray tube. Part II.
1219 X-ray production and filtration in x-ray targets. *Medical Physics* **34**, 2175-2186,
1220 doi:https://doi.org/10.1118/1.2734726 (2007).
1221 69 Meganck, J. A. & Liu, B. Dosimetry in Micro-computed Tomography: a Review of the
1222 Measurement Methods, Impacts, and Characterization of the Quantum GX Imaging
1223 System. *Mol Imaging Biol* **19**, 499-511, doi:10.1007/s11307-016-1026-x (2017).
1224

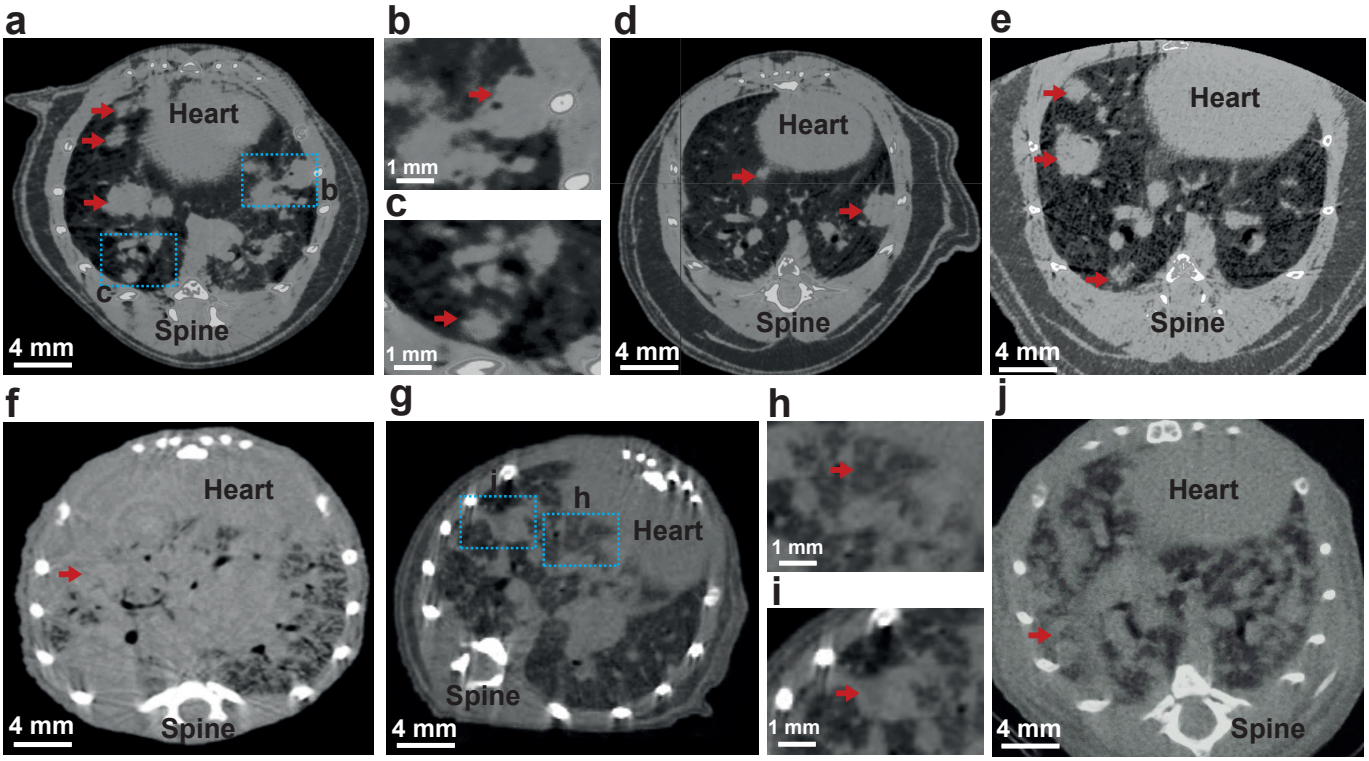
a
Heart
b
c
Spine
4 mm
b
1 mm
c
1 mm
d
Heart
Spine
4 mm
e
Heart
Spine
4 mm
f
Heart
Spine
4 mm
g
j
h
Heart
Spine
4 mm
h
1 mm
i
1 mm
j
Heart
Spine
4 mm

Image acquisition & optimisation (Steps 1-17)

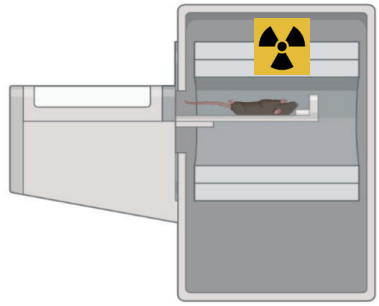

Characterisation & detection of lung tumours (Steps 18-22)

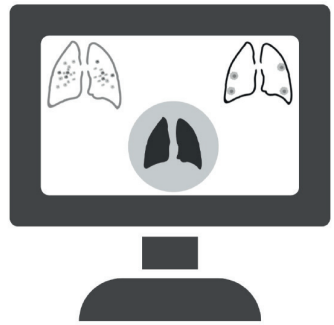

Image analysis & volume quantification (Steps 23-28)

Localised nodules

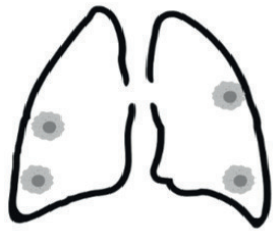

Tumour volume analysis (individual or total nodules)

Diffuse nodules

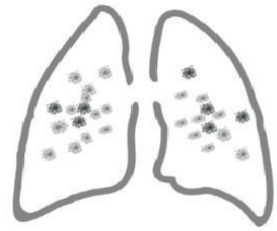

Lung volume analysis

3D volume rendering (Optional)

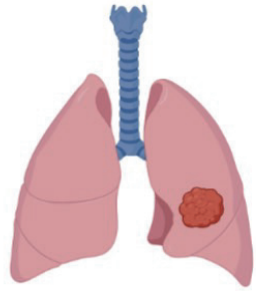

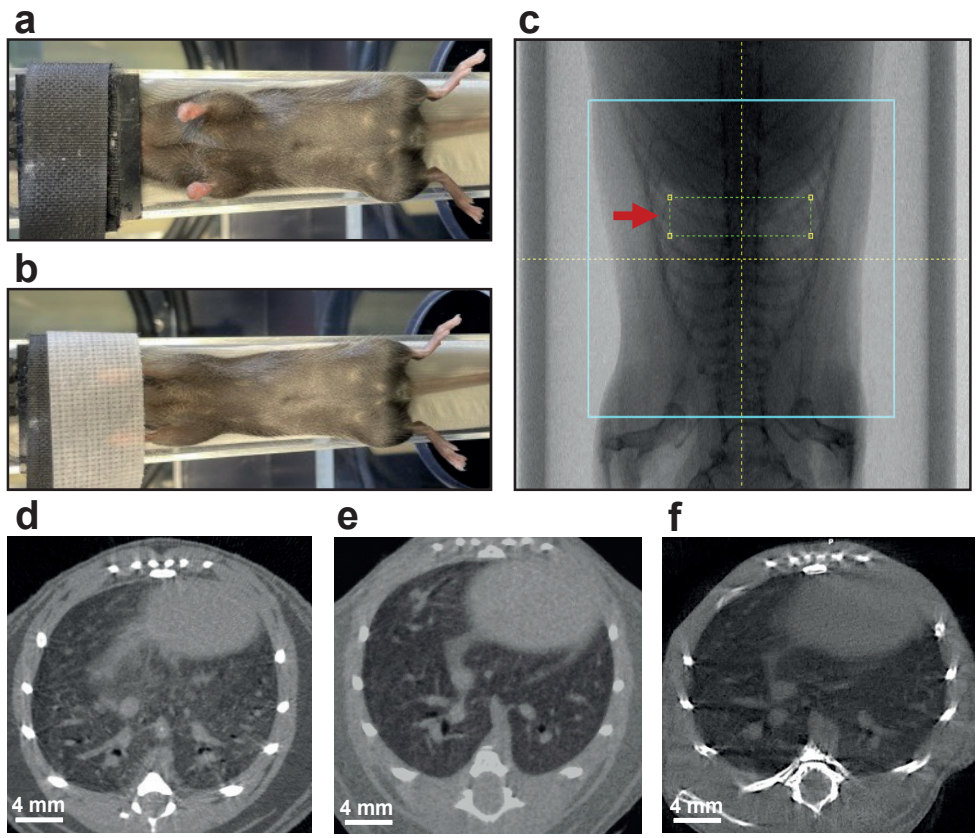
a
b
c
d
e
f
4 mm
4 mm
4 mm

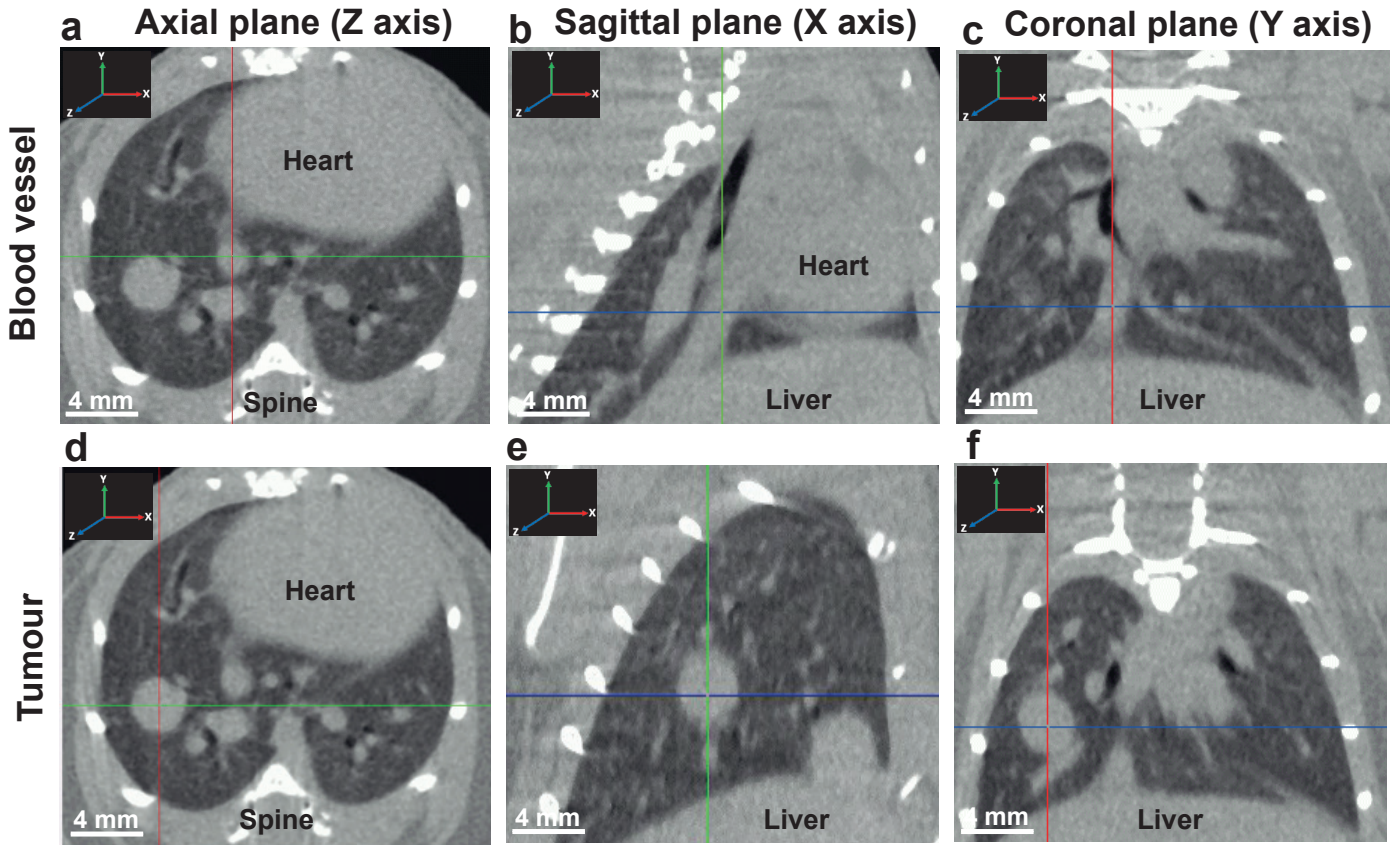
a
Axial plane (Z axis)
b
Sagittal plane (X axis)
c
Coronal plane (Y axis)
Blood vessel
Tumour
Heart
Spine
Liver
4 mm
d
e
f

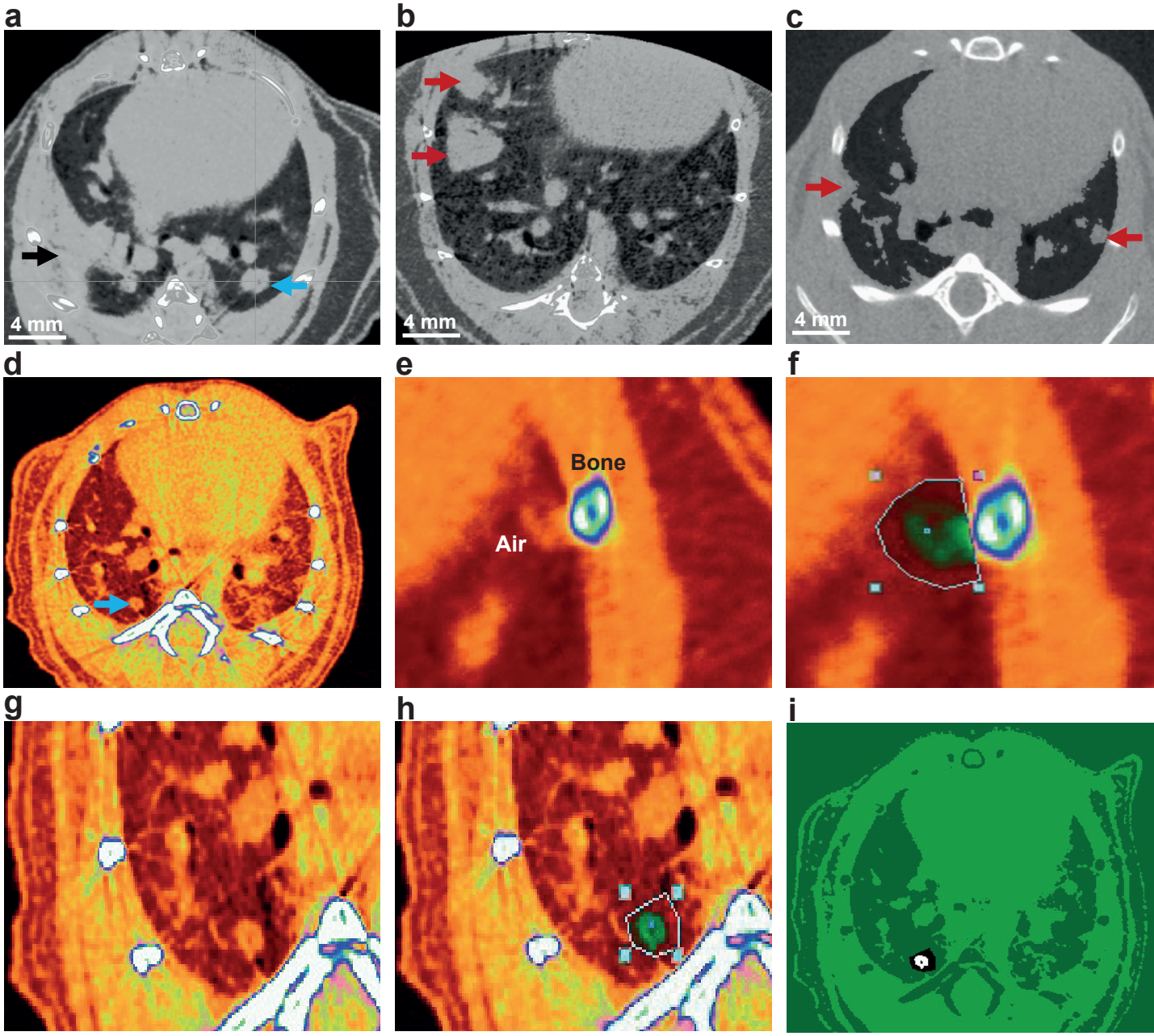
a
b
c
4 mm
4 mm
4 mm
d
e
f
Bone
Air
g
h
i

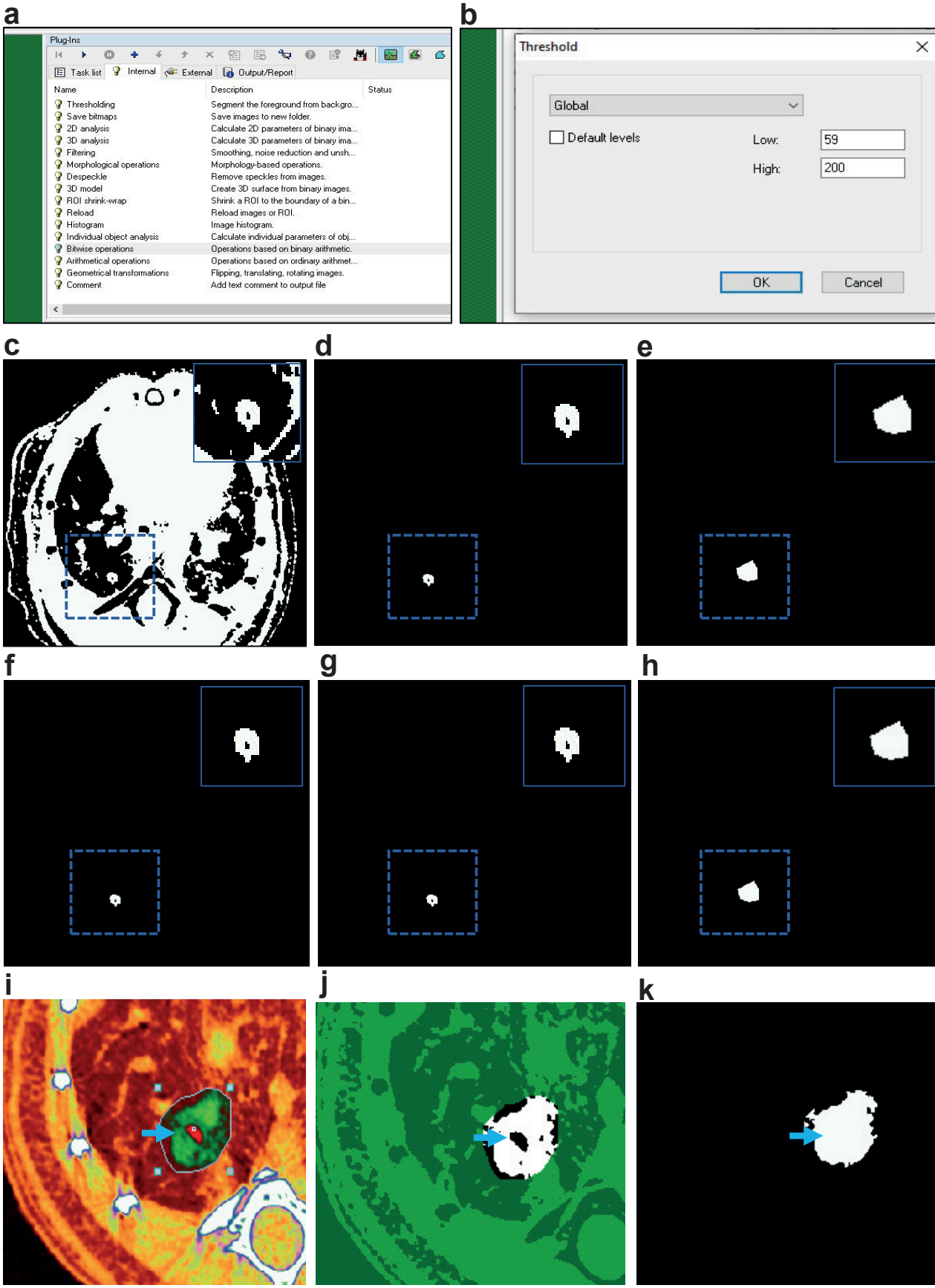
a
Plug-Ins
Task list
Internal
External
Output/Report
Name
Description
Status
Thresholding
Segment the foreground from backgro...
Save bitmaps
Save images to new folder.
2D analysis
Calculate 2D parameters of binary ima...
3D analysis
Calculate 3D parameters of binary ima...
Filtering
Smoothing, noise reduction and unsh...
Morphological operations
Morphology-based operations.
Despeckle
Remove speckles from images.
3D model
Create 3D surface from binary images.
ROI shrink-wrap
Shrink a ROI to the boundary of a bin...
Reload
Reload images or ROI.
Histogram
Image histogram.
Individual object analysis
Calculate individual parameters of obj...
Bitwise operations
Operations based on binary arithmetic.
Arithmetical operations
Operations based on ordinary arithmet...
Geometrical transformations
Flipping, translating, rotating images.
Comment
Add text comment to output file
b
Threshold
Global
Default levels
Low:
59
High:
200
OK
Cancel
c
d
e
f
g
h
i
j
k

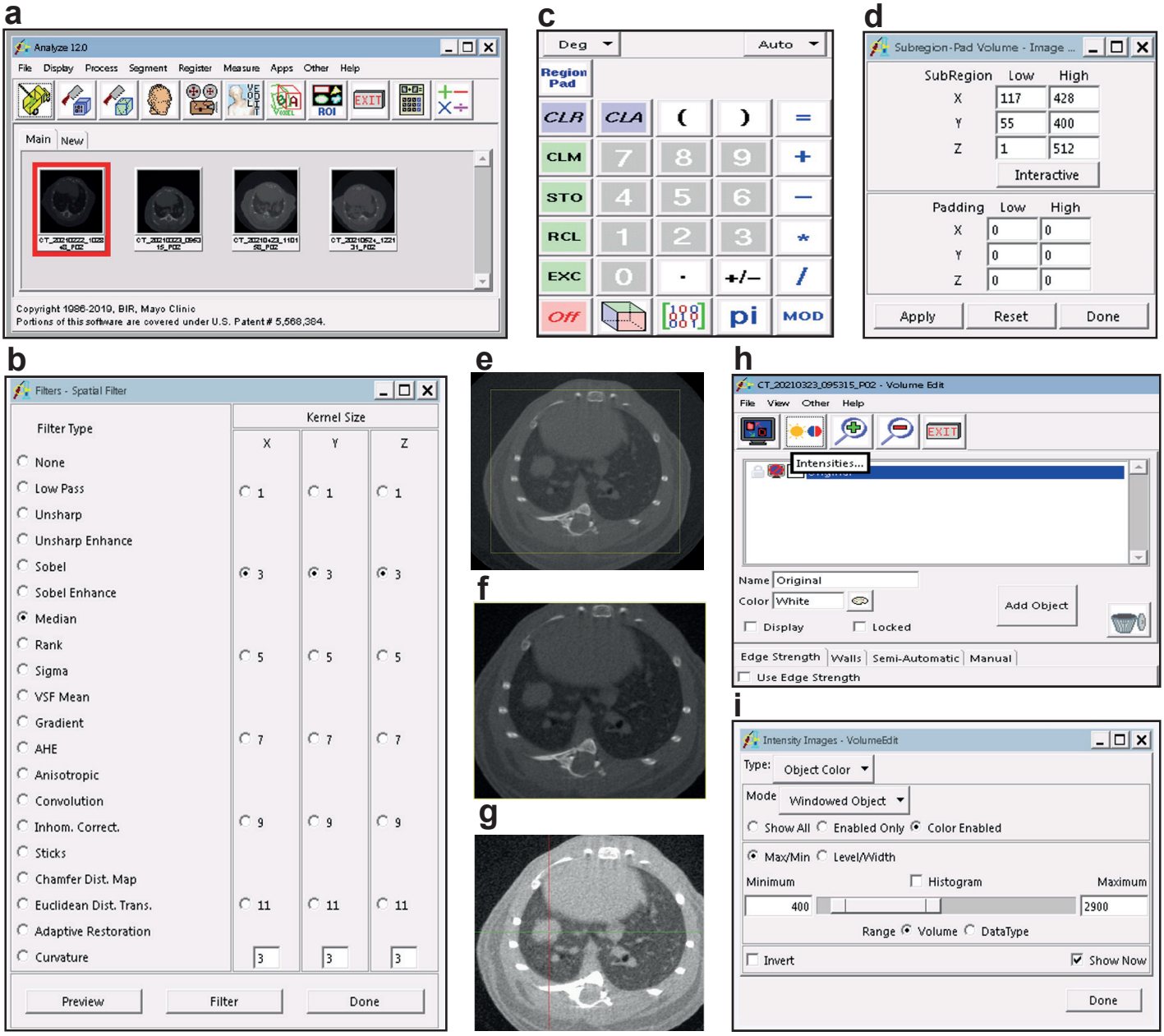
a
Analyze 12.0
File Display Process Segment Register Measure Apps Other Help
ROI
EXIT
Main New
Copyright 1986-2019, BIR, Mayo Clinic
Portions of this software are covered under U.S. Patent # 5,568,384.
c
Deg
Auto
Region Pad
CLR CLA ( ) =
CLM 7 8 9 +
STO 4 5 6 −
RCL 1 2 3 *
EXC 0 . +/− /
Off pi MOD
d
Subregion-Pad Volume - Image ...
SubRegion Low High
X 117 428
Y 55 400
Z 1 512
Interactive
Padding Low High
X 0 0
Y 0 0
Z 0 0
Apply Reset Done
b
Filters - Spatial Filter
Filter Type
Kernel Size
X Y Z
None
Low Pass 1 1 1
Unsharp
Unsharp Enhance
Sobel 3 3 3
Sobel Enhance
Median
Rank 5 5 5
Sigma
VSF Mean
Gradient 7 7 7
AHE
Anisotropic
Convolution
Inhom. Correct. 9 9 9
Sticks
Chamfer Dist. Map
Euclidean Dist. Trans. 11 11 11
Adaptive Restoration
Curvature 3 3 3
Preview Filter Done
e
f
g
h
CT_20210323_095315_P02 - Volume Edit
File View Other Help
EXIT
Intensities...
Name Original
Color White
Add Object
Display Locked
Edge Strength Walls Semi-Automatic Manual
Use Edge Strength
i
Intensity Images - VolumeEdit
Type: Object Color
Mode Windowed Object
Show All Enabled Only Color Enabled
Max/Min Level/Width
Minimum Histogram Maximum
400 2900
Range Volume DataType
Invert Show Now
Done

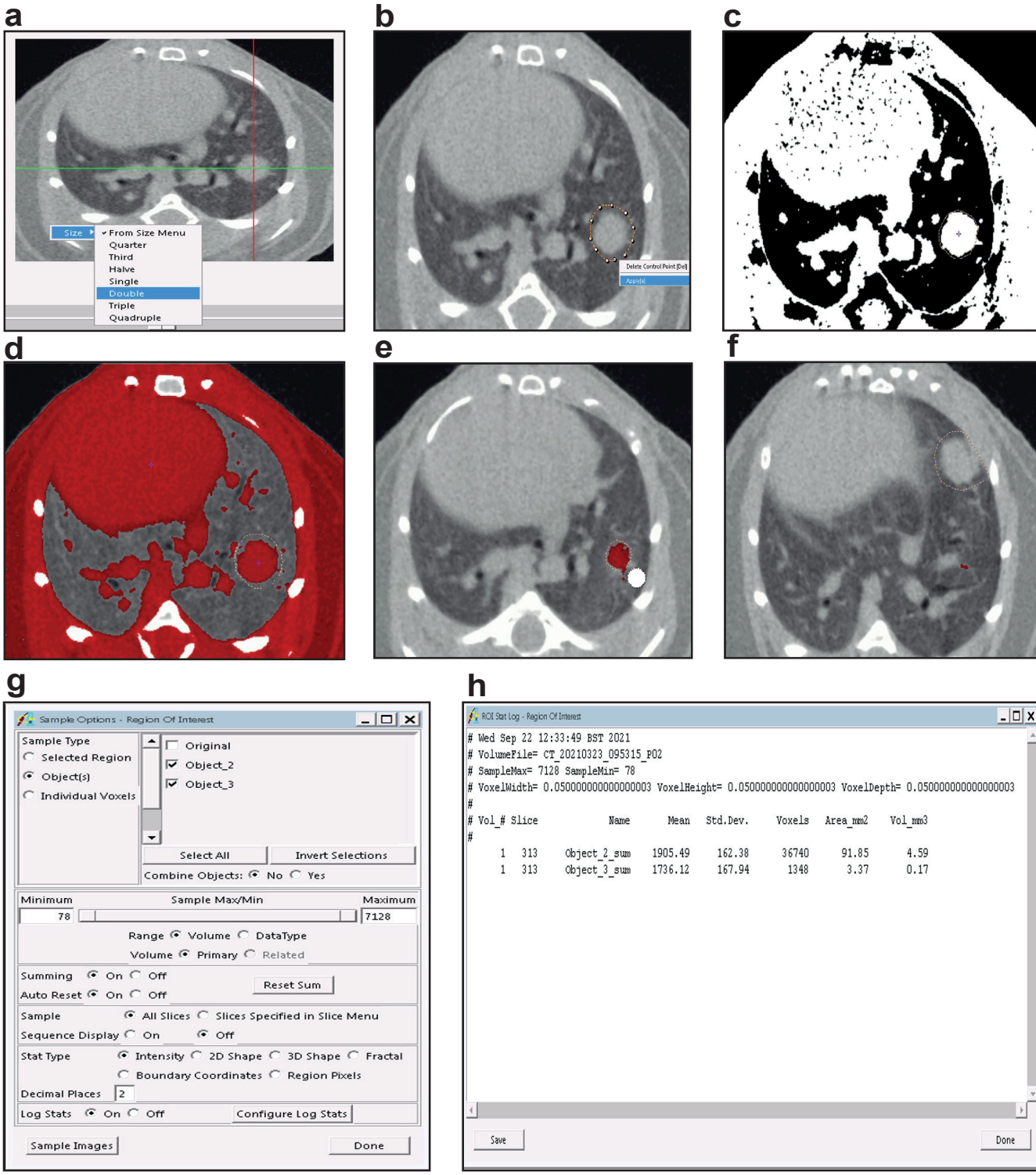
a
Size
From Size Menu
Quarter
Third
Halve
Single
Double
Triple
Quadruple
b
Delete Control Point [Del]
Apply[a]
c
d
e
f
g
Sample Options - Region Of Interest
Sample Type
Selected Region
Object(s)
Individual Voxels
Original
Object_2
Object_3
Select All
Invert Selections
Combine Objects: No Yes
Minimum
Sample Max/Min
Maximum
78
7128
Range Volume DataType
Volume Primary Related
Summing On Off
Auto Reset On Off
Reset Sum
Sample All Slices Slices Specified in Slice Menu
Sequence Display On Off
Stat Type Intensity 2D Shape 3D Shape Fractal
Boundary Coordinates Region Pixels
Decimal Places 2
Log Stats On Off
Configure Log Stats
Sample Images
Done
h
ROI Stat Log - Region Of Interest
Wed Sep 22 12:33:49 BST 2021
VolumeFile= CT_20210323_095315_P02
SampleMax= 7128 SampleMin= 78
VoxelWidth= 0.050000000000000003 VoxelHeight= 0.050000000000000003 VoxelDepth= 0.050000000000000003
#
Vol_# Slice Name Mean Std.Dev. Voxels Area_mm2 Vol_mm3
#
1 313 Object_2_sum 1905.49 162.38 36740 91.85 4.59
1 313 Object_3_sum 1736.12 167.94 1348 3.37 0.17
Save
Done

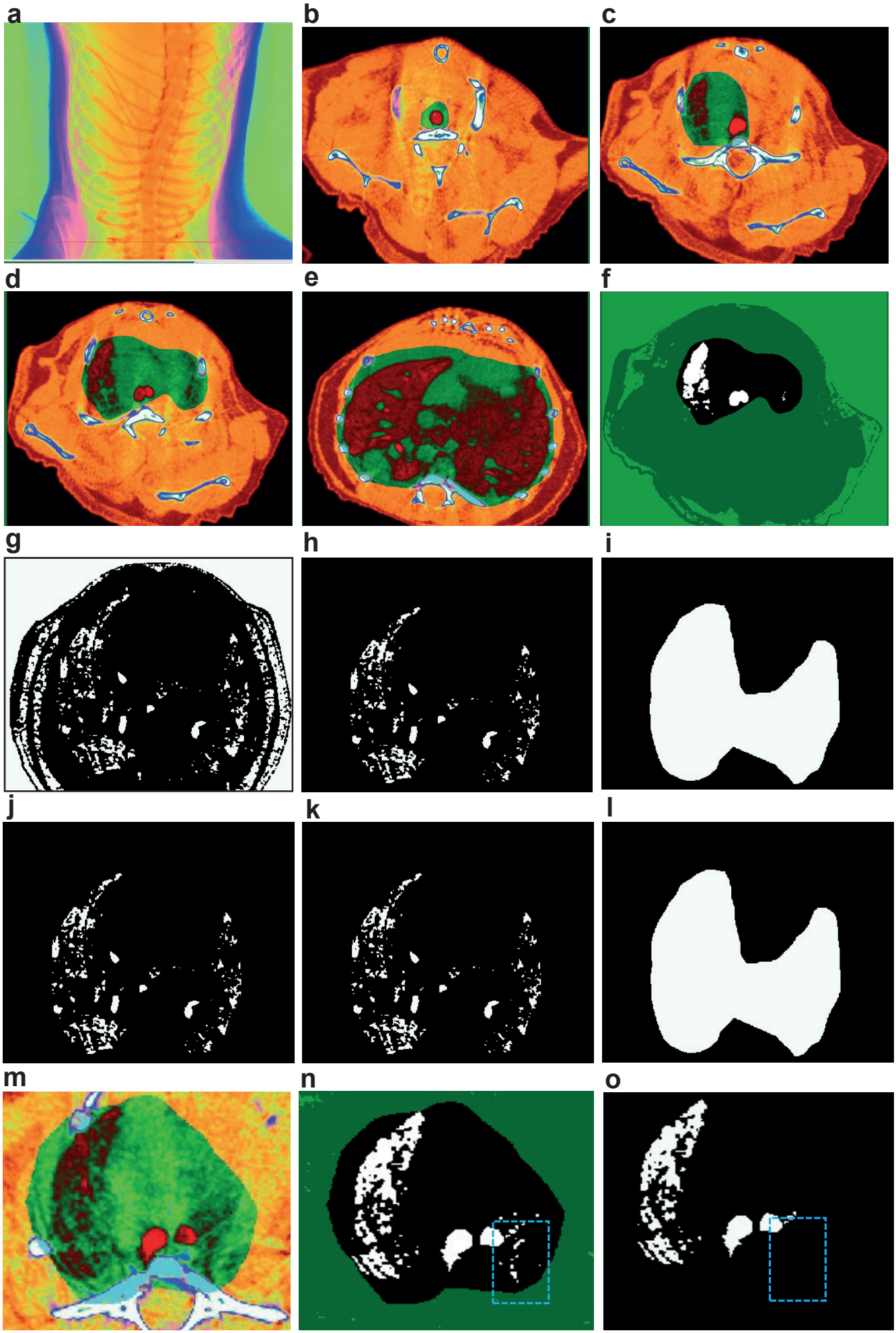
a
b
c
d
e
f
g
h
i
j
k
l
m
n
o

a

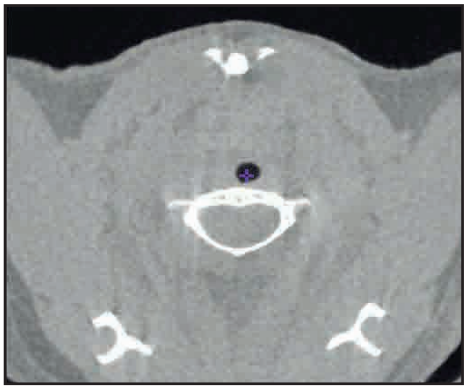

b

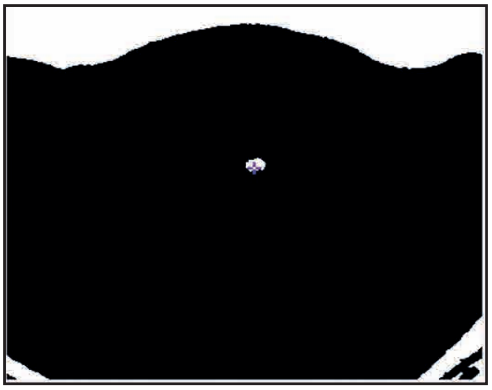

c

d

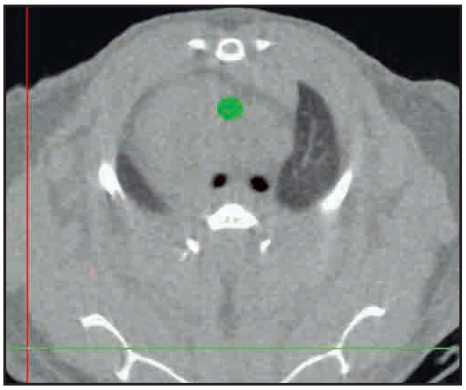

e

f

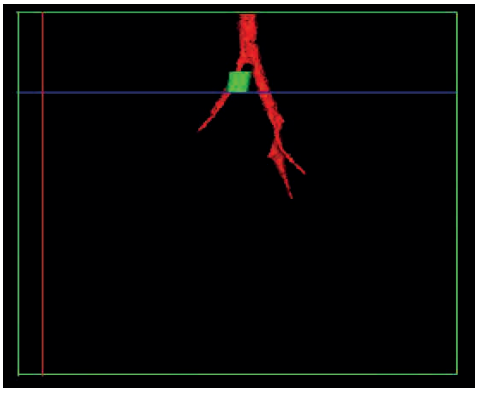

g

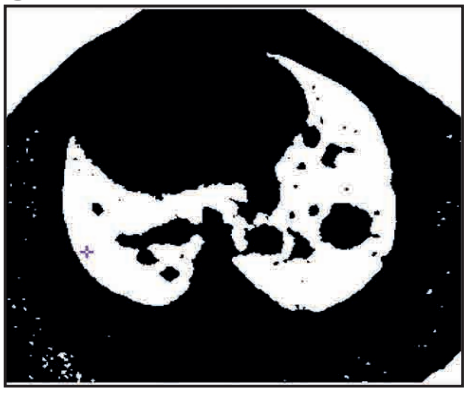

h

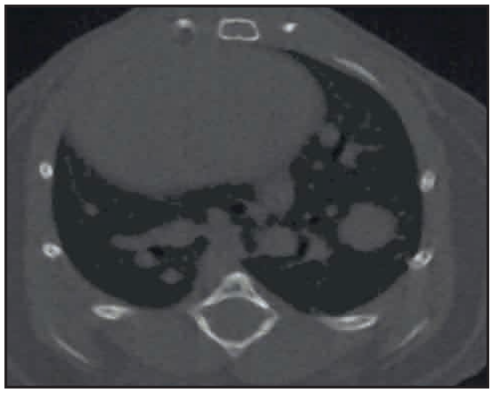

i

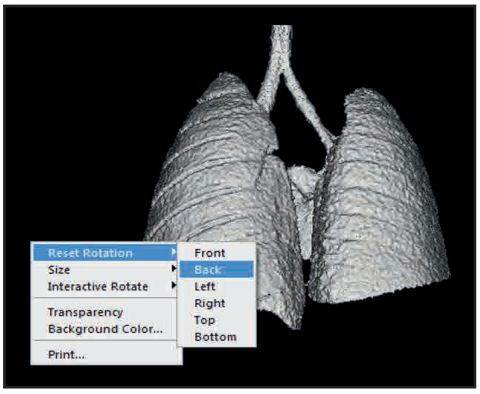

j

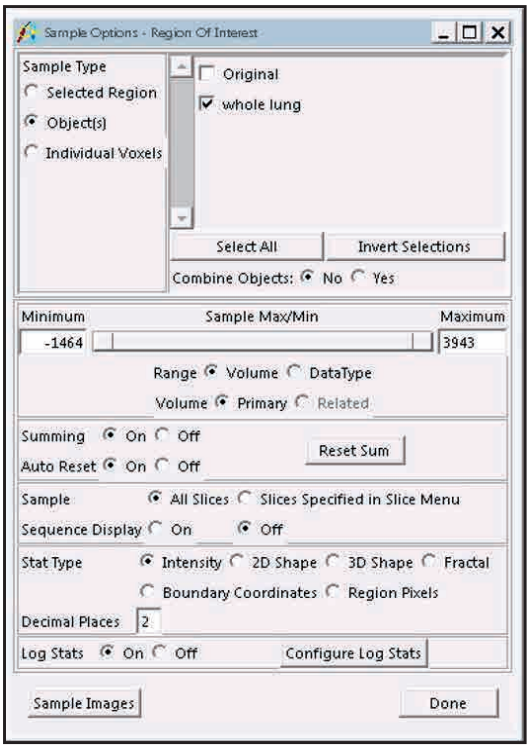

k

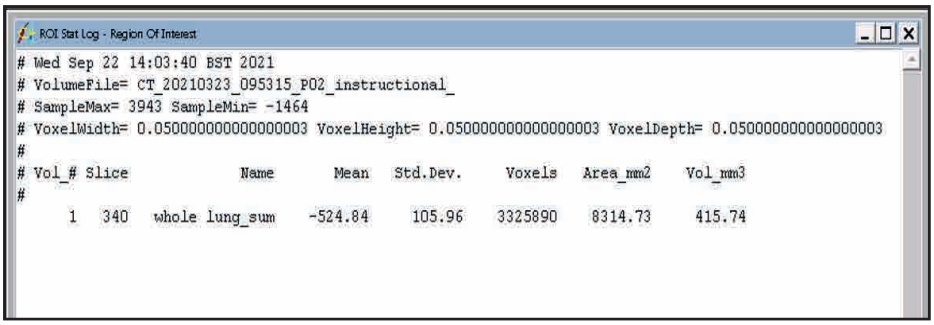

l

Name	Mean HU	Std.Dev.	Vol_mm3	%change	Actual lung volume
whole lung	-524.84	105.96	415.74	0.52484	218.20
				(=Mean*-0.001)	(=Vol_mm3*%change)

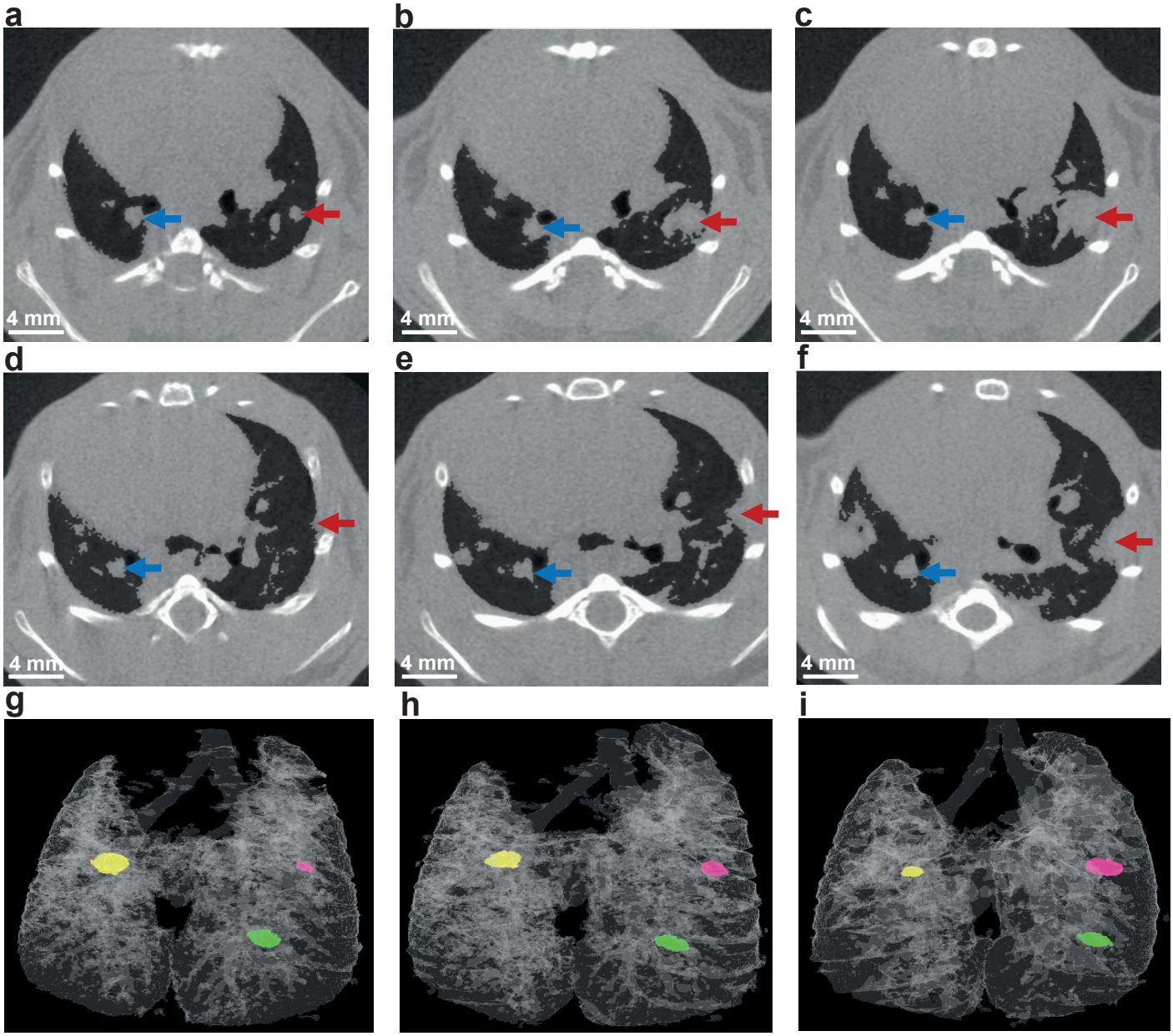
a
b
c
d
e
f
g
h
i
4 mm
4 mm
4 mm
4 mm
4 mm
4 mm